








## Article

# Molecular Docking, Bioinformatic Analysis, and Experimental Verification for the Effect of Naringin on ADHD: Possible Inhibition of GSK-3 $\beta$ and HSP90

Hatem I. Mokhtar <sup>1</sup>, Sawsan A. Zaitone <sup>2,3,\*</sup>, Karima El-Sayed <sup>4</sup>, Rehab M. Lashine <sup>5</sup>, Nada Ahmed <sup>6</sup>, Suzan M. M. Moursi <sup>7</sup>, Shaimaa A. Shehata <sup>8</sup>, Afaf A. Aldahish <sup>9</sup>, Mohamed A. Helal <sup>10,11</sup>, Mohamed K. El-Kherbetawy <sup>12</sup>, Manal S. Fawzy <sup>13</sup> and Noha M. Abd El-Fadeal <sup>14,15</sup>

- <sup>1</sup> Department of Pharmaceutical Chemistry, Faculty of Pharmacy, Sinai University-Kantara Branch, Ismailia 41636, Egypt; hatem.mokhtar@su.edu.eg
- <sup>2</sup> Department of Pharmacology & Toxicology, Faculty of Pharmacy, University of Tabuk, Tabuk 47713, Saudi Arabia
- <sup>3</sup> Department of Pharmacology & Toxicology, Faculty of Pharmacy, Suez Canal University, Ismailia 41522, Egypt
- <sup>4</sup> Medical Physiology Department, Faculty of Medicine, Suez Canal University, Ismailia 41522, Egypt
- <sup>5</sup> Clinical Pharmacology Department, Faculty of Medicine, Suez Canal University, Ismailia 41522, Egypt
- <sup>6</sup> Department of Clinical Pathology, Faculty of Medicine, Suez Canal University, Ismailia 41522, Egypt
- <sup>7</sup> Medical Physiology Department, Faculty of Medicine, Zagazig University, Zagazig 44519, Egypt
- <sup>8</sup> Department of Forensic Medicine and Clinical Toxicology, Faculty of Medicine, Suez Canal University, Ismailia 41522, Egypt
- <sup>9</sup> Department of Pharmacology, College of Pharmacy, King Khalid University, Abha 61441, Saudi Arabia; adahesh@kku.edu.sa
- <sup>10</sup> Biomedical Sciences Program, University of Science and Technology, Zewail City of Science and Technology, October Gardens, 6th of October, Giza 12587, Egypt; mohamed.hilal@pharm.suez.edu.eg
- <sup>11</sup> Medicinal Chemistry Department, Faculty of Pharmacy, Suez Canal University, Ismailia 41522, Egypt
- <sup>12</sup> Department of Pathology, Faculty of Medicine, Suez Canal University, Ismailia 41522, Egypt; mohamed\_elkherbetawy@med.suez.edu.eg
- <sup>13</sup> Department of Biochemistry, Faculty of Medicine, Northern Border University, Arar 91431, Saudi Arabia; manal.darwish@nbu.edu.sa
- <sup>14</sup> Medical Biochemistry and Molecular Biology Department, Faculty of Medicine, Suez Canal University, Ismailia 41522, Egypt
- <sup>15</sup> Biochemistry Department, Ibn Sina National College for Medical Studies, Jeddah 22421, Saudi Arabia
- \* Correspondence: szaitone@ut.edu.sa or sawsan\_zaytoon@pharm.suez.edu.eg



**Citation:** Mokhtar, H.I.; Zaitone, S.A.; El-Sayed, K.; Lashine, R.M.; Ahmed, N.; Moursi, S.M.M.; Shehata, S.A.; Aldahish, A.A.; Helal, M.A.; El-Kherbetawy, M.K.; et al. Molecular Docking, Bioinformatic Analysis, and Experimental Verification for the Effect of Naringin on ADHD: Possible Inhibition of GSK-3 $\beta$  and HSP90. *Pharmaceuticals* **2024**, *17*, 1436. <https://doi.org/10.3390/ph17111436>

Academic Editor: Gunnar P. H. Dietz

Received: 22 September 2024

Revised: 16 October 2024

Accepted: 23 October 2024

Published: 26 October 2024



**Copyright:** © 2024 by the authors. Licensee MDPI, Basel, Switzerland. This article is an open access article distributed under the terms and conditions of the Creative Commons Attribution (CC BY) license (<https://creativecommons.org/licenses/by/4.0/>).

**Abstract: Background/Objectives:** One of the most abundant and growing neurodevelopmental disorders in recent decades is attention deficit hyperactivity disorder (ADHD). Many trials have been performed on using drugs for the improvement of ADHD signs. This study aimed to detect the possible interaction of naringin with Wnt/ $\beta$ -catenin signaling and its putative anti-inflammatory and protective effects in the mouse ADHD model based on bioinformatic, behavioral, and molecular investigations. Furthermore, molecular docking was applied to investigate possible interactions with the GSK-3 $\beta$  and HSP90 proteins. **Methods:** Male Swiss albino mice were divided into four groups, a normal control group, monosodium glutamate (SGL) control, SGL + naringin 50 mg/kg, and SGL + naringin 100 mg/kg. The psychomotor activity of the mice was assessed using the self-grooming test, rope crawling test, and attentional set-shifting task (ASST). In addition, biochemical analyses were performed using brain samples. **Results:** The results of the SGL group showed prolonged grooming time (2.47-folds), a lower percentage of mice with successful crawling on the rope (only 16.6%), and a higher number of trials for compound discrimination testing in the ASST (12.83  $\pm$  2.04 trials versus 5.5  $\pm$  1.88 trials in the normal group). Treatment with naringin (50 or 100 mg per kg) produced significant shortening in the grooming time (31% and 27% reductions), as well as a higher percentage of mice succeeding in crawling with the rope (50% and 83%, respectively). Moreover, the ELISA assays indicated decreased dopamine levels (0.36-fold) and increased TNF- $\alpha$  (2.85-fold) in the SGL control group compared to the normal mice, but an improvement in dopamine level was observed in the naringin (50 or 100 mg per kg)-treated groups (1.58-fold and 1.97-fold). Similarly, the PCR test showed significant declines in the expression of the Wnt (0.36), and  $\beta$ -catenin

(0.33) genes, but increased caspase-3 (3.54-fold) and BAX (5.36-fold) genes in the SGL group; all these parameters were improved in the naringin 50 or 100 mg/kg groups. Furthermore, molecular docking indicated possible inhibition for HSP90 and GSK-3 $\beta$ . **Conclusions:** Overall, we can conclude that naringin is a promising agent for alleviating ADHD symptoms, and further investigations are required to elucidate its mechanism of action.

**Keywords:** ADHD; mouse; monosodium glutamate; naringin; Wnt/ $\beta$ -catenin signaling; molecular docking

## 1. Introduction

Attention deficit hyperactivity disorder (ADHD) is a juvenile neurological illness affecting approximately 2.5% of children, with many individuals continuing to exhibit symptoms into adulthood [1,2]. The condition is characterized by behaviors that disrupt social interactions, including hyperactivity, impulsiveness, and inattention, which can significantly impact educational outcomes and personal development [3]. Environmental factors such as hypoxia during prenatal life may also play a role in the development of ADHD [4]. Evidence from imaging, clinical, and experimental studies documented the involvement of catecholamine dysregulations in ADHD. For example, amplified dopamine transporter binding was observed in ADHD patients [5,6], and reduced noradrenaline transporter expression in specific brain regions [7].

Recent studies have highlighted the significance of protein targets such as heat shock protein 90 (HSP90) and glycogen synthase kinase 3 beta (GSK-3 $\beta$ ) in the context of neurodevelopmental disorders, including ADHD [8,9]. HSP90 is involved in the regulation of various signaling pathways and is crucial for the stabilization and proper functioning of several proteins involved in neurotransmission [10]. Dysregulation of HSP90 has been linked to neurodevelopmental disorders, suggesting its potential role in the pathophysiology of ADHD [8]. Recent studies showed that HSP90 inhibition prevented neuronal cell loss [11,12] and rescue synaptic dysfunction in animal models of neurodegeneration [13]. Further, HSP inhibition protects against retinal degeneration in rats [14] and open-angle glaucoma [15].

Additionally, GSK-3 $\beta$  is known to be involved in neurodevelopment and synaptic plasticity; its dysregulation can impact dopamine signaling and is implicated in the clinical manifestations of ADHD [16,17]. These findings provide a compelling rationale for exploring interventions that target these proteins in the context of ADHD. Exposure to glycogen synthase kinase 3 (GSK3) inhibitors significantly increased activation of Wnt/ $\beta$ -catenin signaling [18]. Chemical screening efforts have prioritized GSK-3 $\beta$  inhibitors as inducers of cell differentiation [19]. Ruiz and Eldar-Finkelman reviewed the use of GSK-3 inhibitors in CNS disorders [20]. Hence, legends that possess an inhibiting activity against Hsp90 are promising neuroprotectants.

The Wnt/ $\beta$ -catenin is an evolutionarily developmental signaling pathway that plays a crucial role in tissue homeostasis [21]. The Wnt/ $\beta$ -catenin signaling pathway has been associated with the etiology of various diseases, including ADHD [22–24]. Aberrant Wnt signaling may affect neuronal development and function, further contributing to ADHD symptomatology [25].

Psychostimulants such as amphetamine are first-line pharmacotherapies for patients with ADHD [26]. The longer-acting stimulants deliver extended effectiveness, which restricts the need for daily dosing and lessens the social stigma related to taking medications in the school setting. However, they result in side effects and are more costly [27]. The shorter-duration drugs require high compliance, since they should be taken 2–3 times a day [28]. On the other hand, non-stimulant drugs have the advantage of reduced liability for substance misuse. For example, atomoxetine has a lower potential for abuse, but its efficacy is lower than stimulants. Atomoxetine carries a warning for increasing suicidal potential

or the development of jaundice or liver injury [28,29]. There are also alpha agonists, such as clonidine and guanfacine, which activate the CNS presynaptic autoreceptor inhibitory function. These drugs have some disadvantages, such as requiring multiple daily doses, and may result in a hypotensive effect [29]. Another drug is bupropion, which works through dopamine and norepinephrine, and we can expect side effects upon its use, such as irritability, anorexia, insomnia, and increased risk for seizures [28]

Monosodium glutamate (SGL) is a common food flavor enhancer agent used on a wide scale [30]. Improper consumption of SGL above the allowed level is documented to raise glutamate blood concentration, cross the blood–brain barrier, and accumulate in CNS tissue [31]. Exaggerated glutamate levels are known as causes of excitotoxicity and are reported to induce many neurodegenerative disorders, including ADHD [32,33]. SGL induces persistent neurotoxic impact by increasing oxidative stress injury, apoptosis, and neurodegeneration [34,35].

Naringin (4',5,7-trihydroxy flavanone 7-rhamnoglucoside) is an abundant flavanone in grapefruit and Citrus species [36,37]. Upon oral administration, naringin hydrolyzes to naringenin. The latter is a major metabolite that can be absorbed easily from the GIT [37]. Naringin can cross the blood–brain barrier [38] and was documented to possess anti-inflammatory, anti-oxidative, and anti-apoptotic properties in rat hippocampi [39]. Naringin has been considered a neuroprotective agent due to the induction of neurotrophic factors [40]. Furthermore, naringin exhibited a neuroprotective effect against neuronal apoptosis through modulation of the Bax and Bcl-2 pathways [41]. Collectively, naringin acts on several neuroprotective antioxidants that function against oxidative neurotoxicity in vitro [42] and hippocampal oxidative neurotoxicity in rats [43]. Further, Ahmed et al. reviewed the therapeutic potential of naringin in neurologic disorders and suggested further study and consideration of this compound as a potential candidate for neurotherapeutics [44].

Currently, there is still an inadequate understanding of the influence of nutraceuticals in alleviating ADHD symptoms. Hence, the current study was designed to investigate the ameliorative effect of naringin on the attentive behavior of an ADHD mouse model induced by SGL. The aim was extended to exploring the possible inhibition of HSP90 and GSK-3 $\beta$  by naringin, leading to increasing Wnt/ $\beta$ -catenin signaling.

## 2. Results

### 2.1. Molecular Docking and Bioinformatic Results

Naringin was docked into the active site of its potential targets, GSK-3 $\beta$  and HSP90. The proposed binding mode of naringin in the active site of GSK-3 $\beta$  (PDB ID: 4AFJ) shows the expected and essential H-bond between the disaccharide moiety and the backbone of Val135 in the hinge region of the kinase [45]. In addition, the aglycone part fits nicely into the large hydrophobic back pocket of the enzyme, making several contacts. As depicted in Figure 1A, these interactions include two strong H-bonds with the catalytic Lys85 and Asn95, and relatively weak contacts with Lys183 and Ser203. It was noticed that the 2-phenyl-chromen-4-one scaffold places the four oxygens in an ideal orientation for these H-bonding interactions. In addition, the phenyl ring of the chromene nucleus forms a close  $\pi$ -stacking interaction with Phe67 at the top of the active site.

Additionally, we docked naringin into the ATP-binding site located centrally in the Hps90-NTD using the crystal structure of the protein in a complex with the potent triazole-based inhibitor, JMC31 (PDB ID: 8AGI) [46]. The disaccharide fragment shows H-bonds with the critical Asp93 and Thr184 in the ATP-binding site (Figure 1B) [46,47]. In addition, the chromene ring fits into the lower hydrophobic pocket, making a  $\pi$ -stacking interaction with Phe138 and favorable hydrophobic contacts with Leu107. Moreover, it is worth noting that the naringin carbonyl lies in close proximity to the critical Lys112, which is essential for binding with ATP, and could be involved in a water-mediated H-bond with this important residue [47]. Further, the phenolic ring of naringin extends into the solvent-exposed pocket in a similar fashion to the cyclohexyl ring of JMC31.

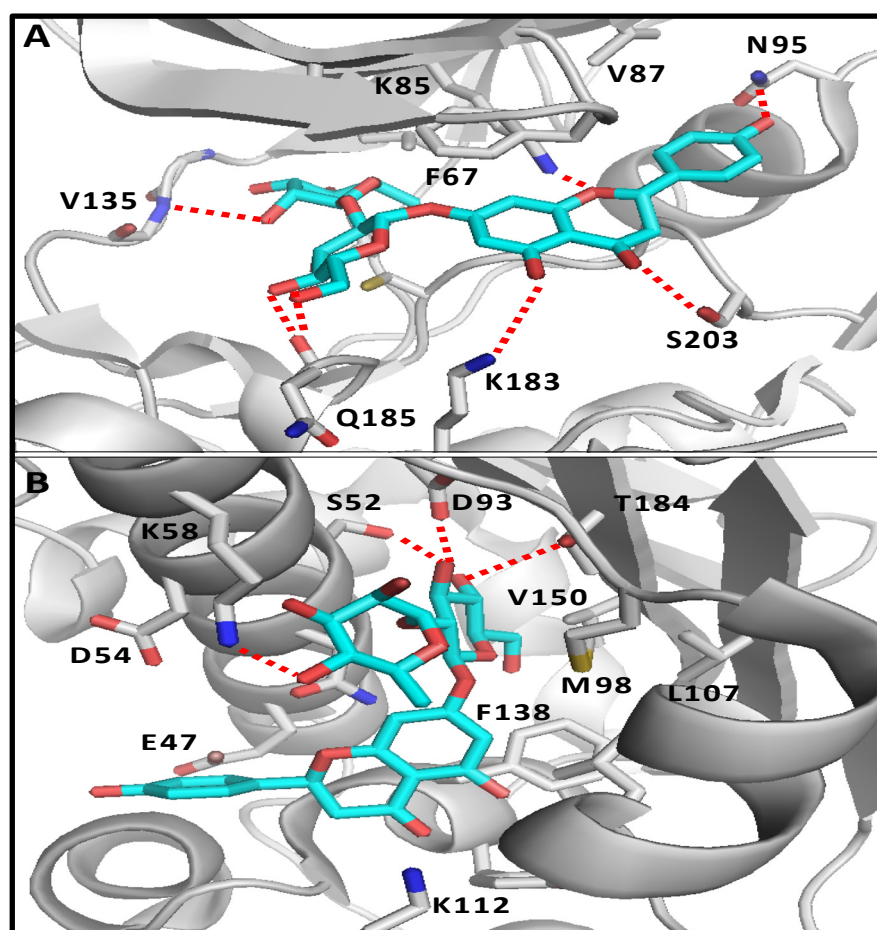


**Figure 1.** Proposed binding mode of naringin in the ATP-binding site of GSK-3 $\beta$  (A) and HSP90 (B). Ligand is displayed as cyan sticks and the important protein residues are displayed as gray sticks with a cartoon backbone. Polar contacts are shown as red dashed lines.

In addition, a molecular dynamics (MD) simulation was performed to study the time-dependent behavior of the complexes and validate the proposed binding modes (Figure 2A). For the naringin-GSK-3 $\beta$  complex, and as evident from the RMSD chart (Figure 2B), the protein backbone slightly fluctuated in the beginning of the simulation and then stabilized after 40 ns, while the ligand showed a significant fluctuation around 40–60 ns and remained stable close to its initial orientation until the end of the simulation run. Figure 2B represents the predominant interactions and their stability during the simulation time. It is evident that the critical H-bond with the hinge region residue Val135 was stable for more than 50% of the MD time, either directly or via a water molecule. Interestingly, the interaction fraction diagram showed H-bonding with Lys85 and Lys183, where the most significant polar contacts contribute to the binding in the hydrophobic pocket and might be responsible for the binding pose stability.

On the other hand, the complex of naringin with HSP90 showed the expected stable H-bonds with Asp93 and Thr184, as described above, with persistent interactions for 96% and 80% of the simulation time, respectively (Figure 3A). The protein backbone and the ligand showed fluctuation at the beginning of the simulation and then stabilized after 40 ns around 3.5 and 5.2 Å, respectively (Figure 3B). To our delight, the overall proposed binding mode was found to become tighter, with the ligand moving deeper into the ATP pocket, facilitated by the strong H-bond anchoring.

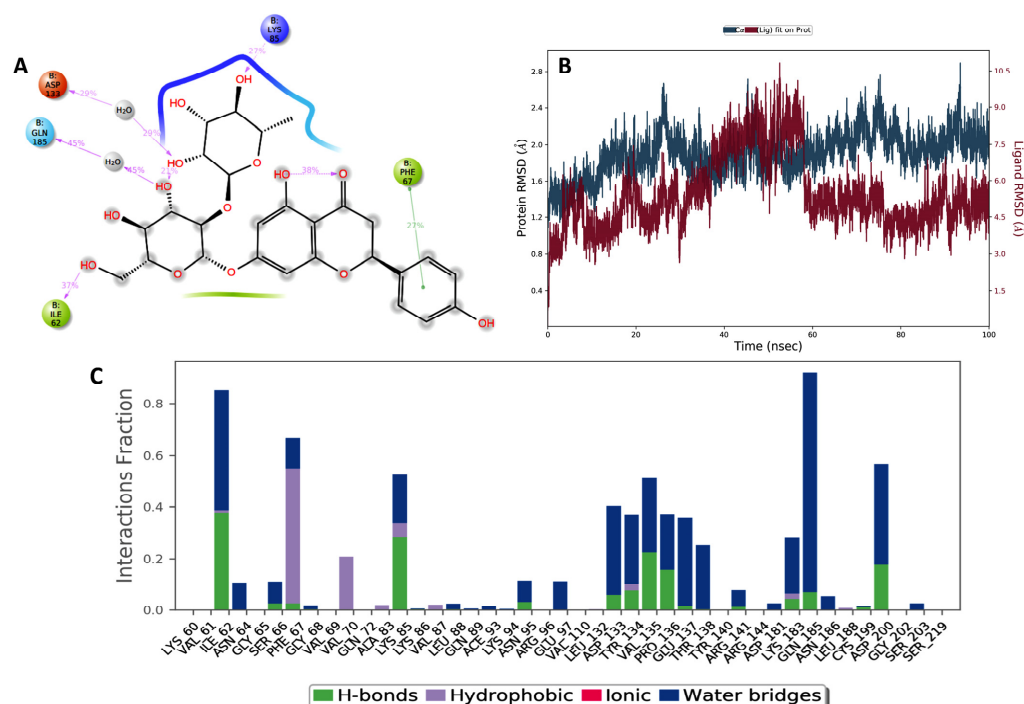


**Figure 2.** (A) Two-dimensional representation of the binding mode of naringin in the ATP-binding site of GSK-3β. The interaction stability over the MD simulation is displayed as a percentage beside each interaction. (B) RMSD of the backbone and the ligand during the MD simulation. (C) Interaction fraction diagram during the 100 ns simulation.

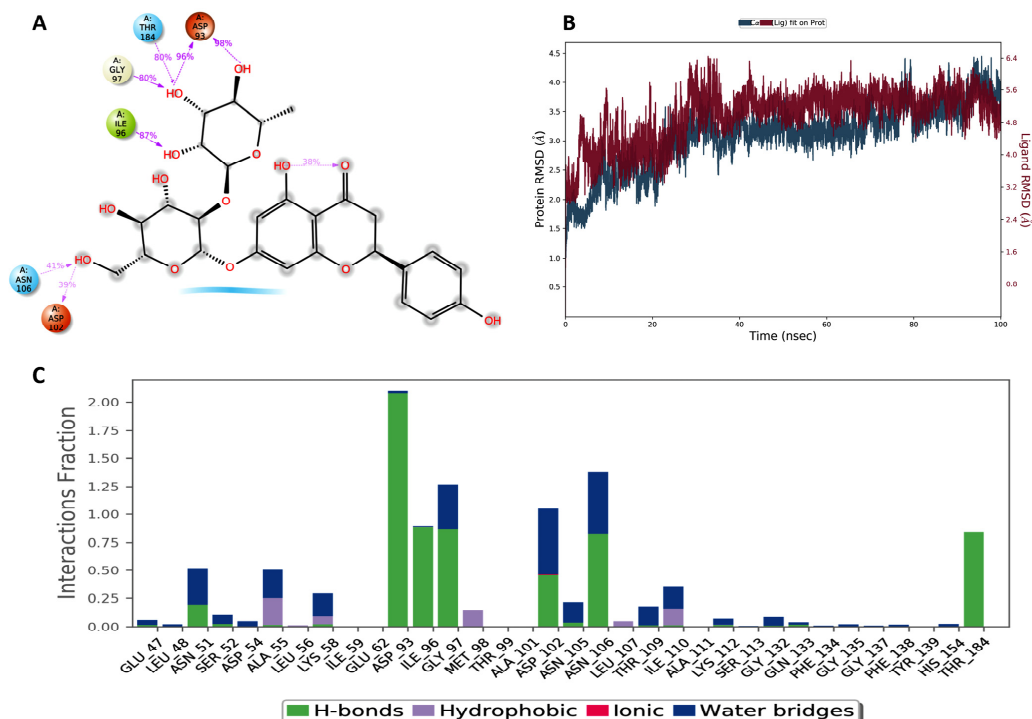


**Figure 3.** (A) Two-dimensional representation of the binding mode of naringin in the ATP-binding site of HSP90. The interaction stability over the MD simulation is displayed as a percentage beside each interaction. (B) RMSD of the backbone and the ligand during the MD simulation. (C) Interaction fraction diagram during the 100 ns simulation.

## 2.2. The Bioinformatic Results

A search was performed on the KEGG pathway for the mechanism of action of naringin and found that the Wnt pathway is involved (map04310). It is known that the Wnt pathway is crucial for some of the morphogen production necessary for basic development. Integration between the naringin mechanism and the canonical Wnt pathway was noticed. Wnt protein inhibits the  $\beta$ -catenin degradation complex and, at this time,  $\beta$ -catenin becomes ready to enter the nucleus and stimulate the Wnt-controlled genes (Figure 4).

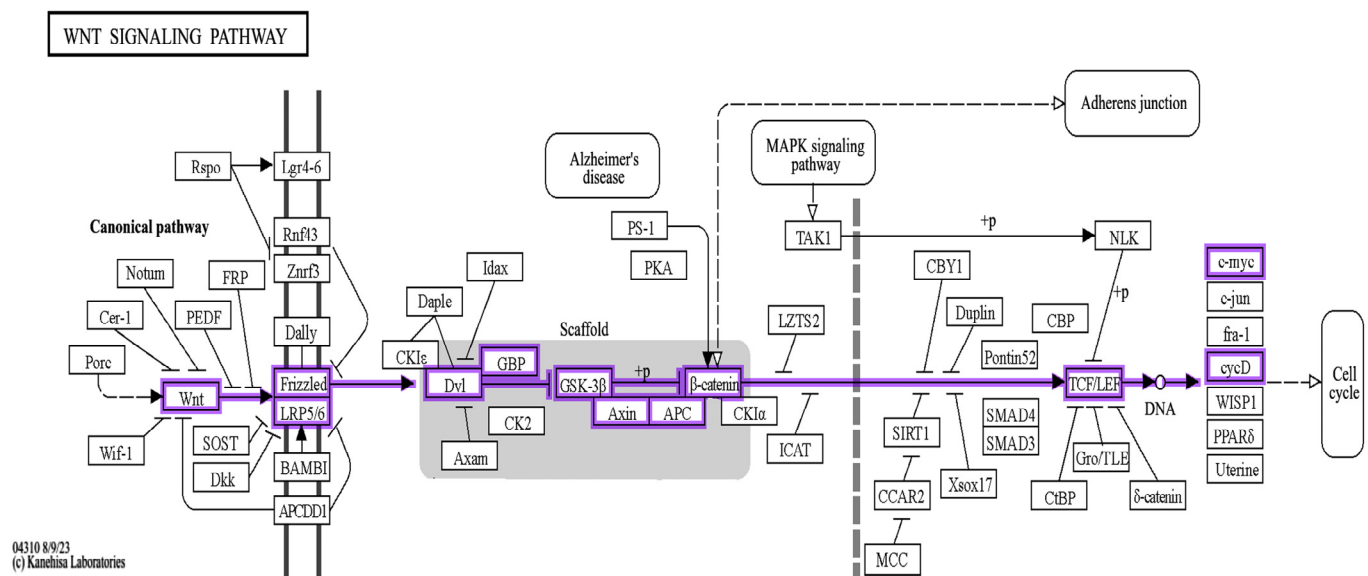


**Figure 4.** Wnt signaling pathway [04310]. The pathway was obtained from the KEGG database and shows that Wnt/ $\beta$ -catenin is involved in the nuclear translocation of  $\beta$ -catenin and the activation of target genes via TCF/LEF transcription factors, making this pathway crucial for the self-renewal of cells.

A STRING database analysis of protein-protein interactions (PPI) reveals that Wnt/ $\beta$ -catenin proteins impact proteins involved in cell cycle regulation and apoptosis through interactions with several proteins, such as GSK-3 $\beta$  and HSP90ab1. These interactions adversely affect various cellular processes, including cell survival. Therefore, controlling the expression levels of these proteins may help to protect cells. The database revealed that the PPI enrichment is highly significant, with a *p*-value of 0.000591 (Figure 5A–D), and the gene ontology molecular process revealed its role in the regulation of neuronal cell maturation and brain development, with an evidence score = 2.47 (Figure 5E).

Furthermore, a dot plot was created for presenting the top fifteen diseases related to the designated target genes determined for naringin (Figure 6A). In addition, the Disease Alliance database was used with an FDR cutoff value of 0.05. Cognitive disorders, such as PD and AD, were found to have a strong relation with many of the naringin target genes (Figure 6A). To demonstrate these data, a Venn diagram was plotted using the FunRich 3.1.3 tool (Figure 6B); it shows the shared pathways between naringin and ADHD-related genes. Indeed, thirteen pathways were noticed in common between the naringin-related genes (originally 76) and the ADHD-related pathways (originally 35 pathways). Moreover, a heatmap was made with the aid of the FunRich 3.1.3. tool to present the pattern by which gene expression takes place (Figure 6C).

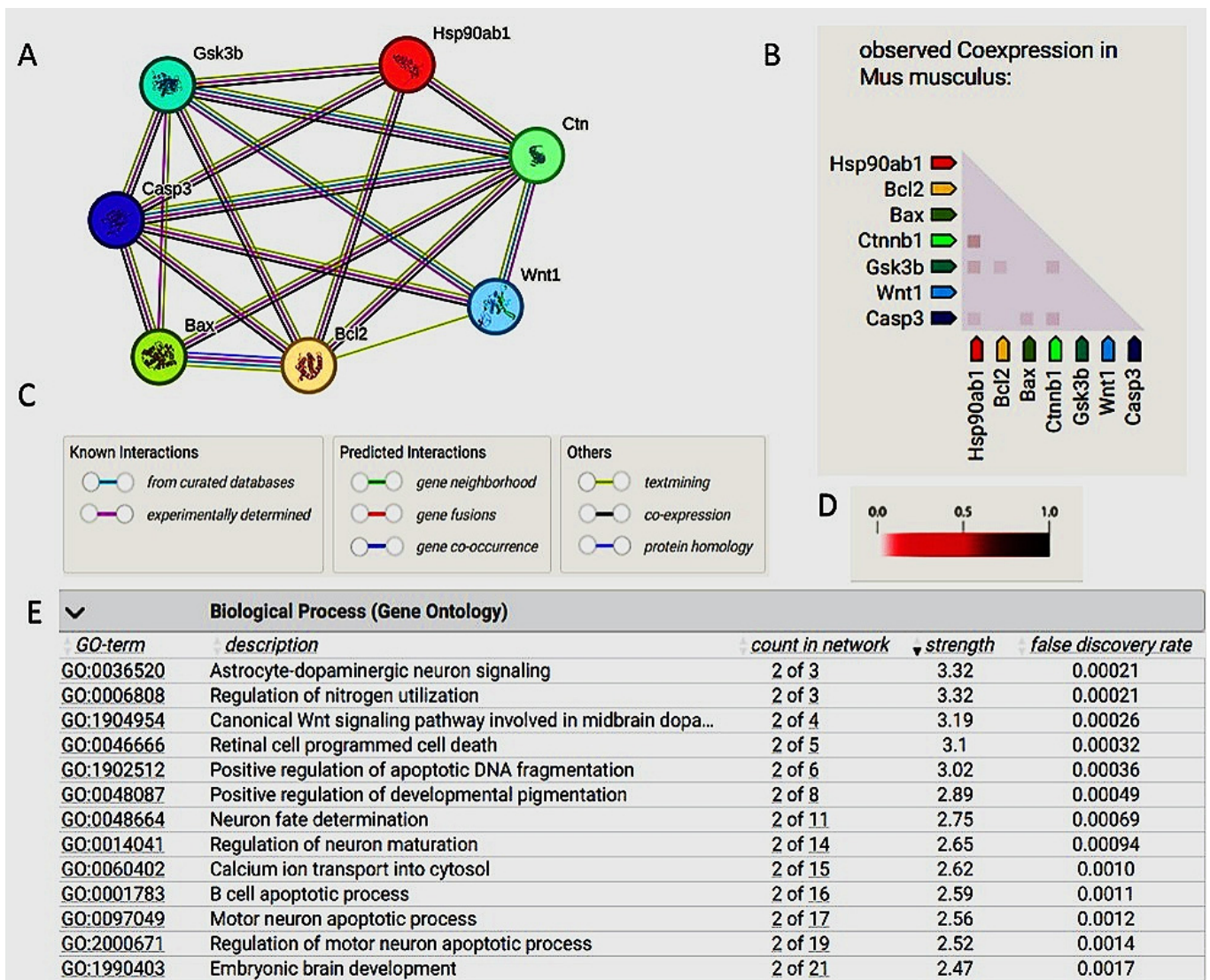


**Figure 5.** Role of Wnt/β-catenin signaling. **(A)** Wnt/β-catenin interactions with many proteins, such as GSK3B, HSP90, Casp3, BAX, and Bcl2. **(B)** Co-expression analysis of interacting proteins. **(C)** The colored lines indicate different evidence types. For example, red is fusion evidence, light blue is a database, green is neighborhood, blue is co-occurrence, purple is experimental evidence, black is co-expression, and yellow is text mining evidence. **(D)** The intensity of the color indicates the level of confidence that two proteins are functionally associated. **(E)** Gene ontology shows the molecular processes most associated with Wnt/β-catenin signaling. Wnt1: proto-oncogen Wnt-1, CASP3: caspase-3 subunit p-12, BAX: apoptosis regulator BAX, BCL2: BCL2-like protein 2, Hsp90ab1: heat shock protein HSP 90-beta1, Ctnnb1: catenin beta-1, Gsk3b: glycogen synthase kinase-3 beta.

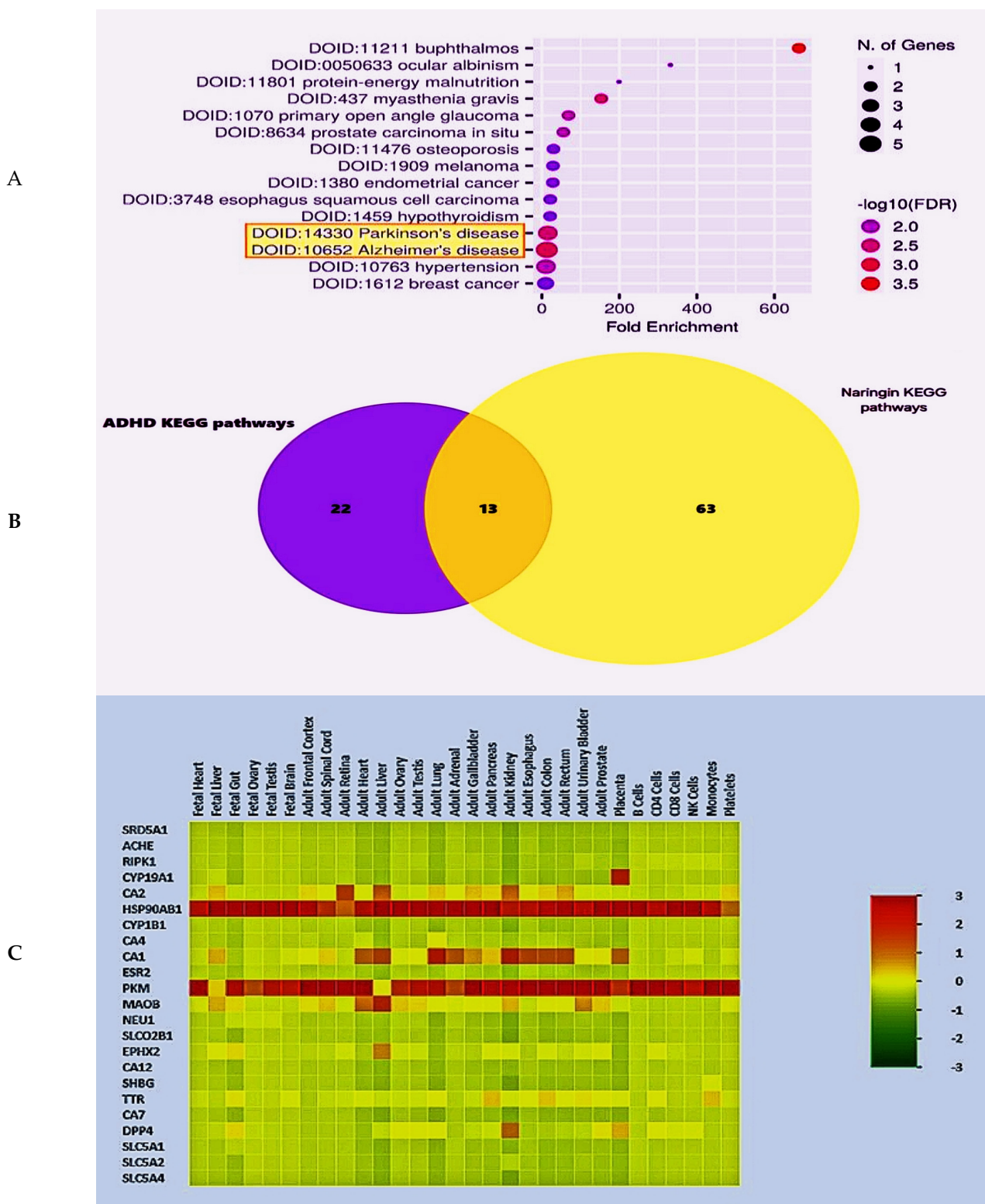


**Figure 6.** (A) A ShinyGo 0.8 dot plot representing the top 15 diseases related to naringin target genes. (B) A Venn diagram showing the target genes of naringin (yellow circle) and ADHD (violet circle) and the common pathways between them (brown part). The diagram was created using FunRich. (C) A heatmap demonstrating the model of gene expression of naringin target genes. The FunRich 3.1.3 bioinformatic tool was used. The color code of the heatmap ranges from 3 to −3, with 3 (most red) being the most expressed and −3 (most green) being the least expressed.



### 2.3. Mouse Study Results

#### 2.3.1. Self-Grooming and Rope Crawling Tests

The results of the self-grooming test indicated a prolongation of the grooming time in the SGL control group. On the other hand, the naringin-50- and naringin-100-treated groups did not show significant shortening in the grooming time, as indicated in Figure 7A. In addition, a low percentage of mice (16.66%) succeeded in crawling with the rope in the SGL control group. However, the naringin-50 and naringin-100 groups demonstrated high percentages of successful mice (50% and 83.33%), as shown in Figure 7B.

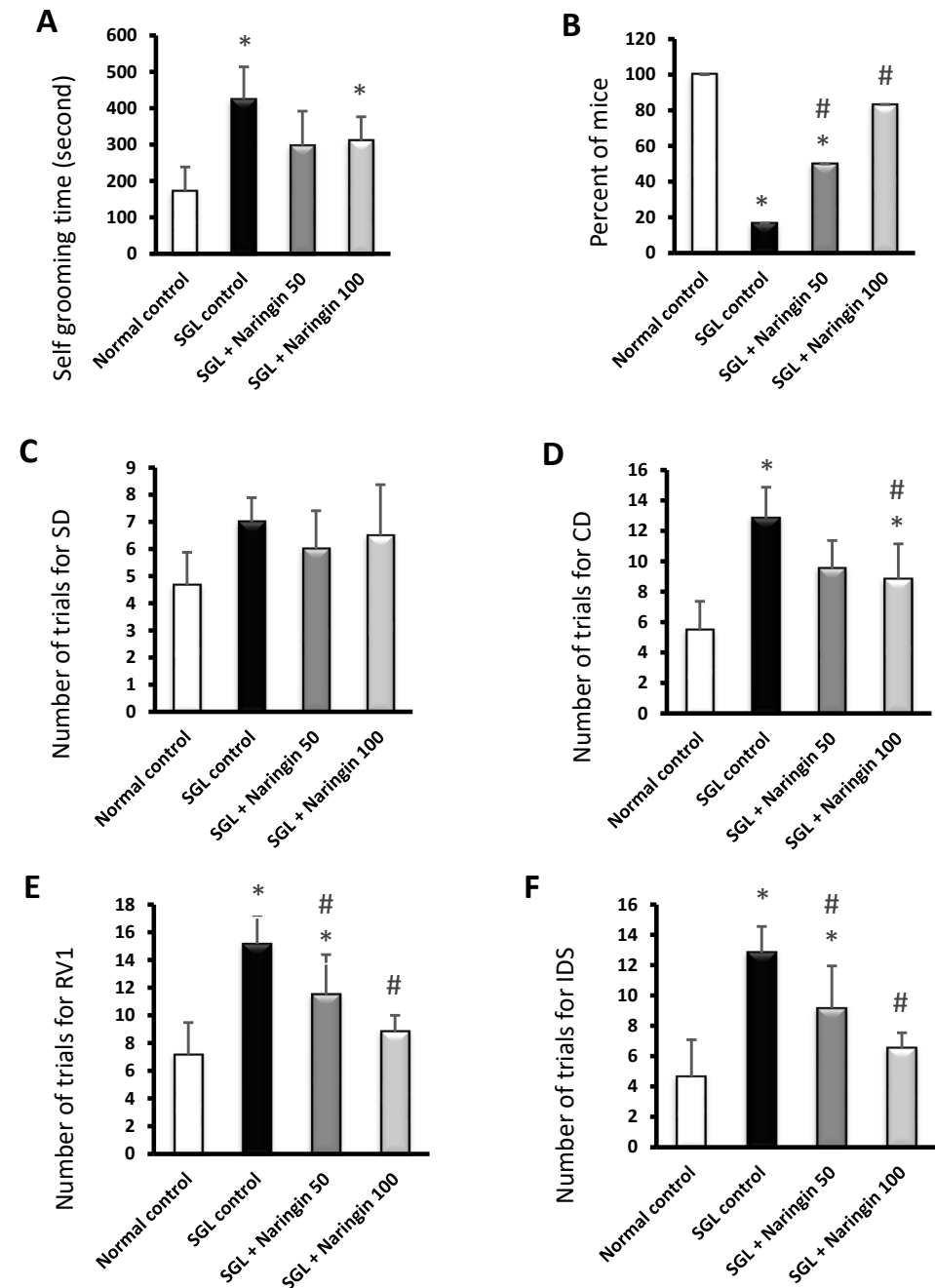


**Figure 7.** The behavior of mice in the self-grooming test and rope crawling test, and the number of trials in ASTT. (A) The time taken for self-grooming. (B) The percentage of mice (out of six) crawling on the rope. (C) The SD phase, (D) the CD phase, (E) the RV1 phase, and (F) the IDS phase. Data are means  $\pm$  SD except for Panel (B), which is the % of animals. At  $p < 0.05$ , \* vs. normal and # vs. SGL control.

### 2.3.2. ASST

In the ASST, the observed numbers of trials for SD were not different among the experimental groups (Figure 7C). The number of trials for CD in the SGL control was larger than in the normal control. The mice in the naringin-100 groups required fewer trials to achieve the CD criteria, as shown in Figure 7D. Further, the SGL control group consumed more RV1 and IDS criteria trials than the normal control group. The naringin-50 and naringin-100 groups showed significant declines in the required trials to achieve RV1 and IDS criteria (Figure 7E,F).

### 2.3.3. ELISA Assays

The current results indicate decreased dopamine content in the brains of the SGL control group compared with the normal control group (Figure 8A). In contrast, increased glutamate levels were observed in the SGL group (Figure 8B). The naringin-treated groups (50 and 100 mg) showed significant improvements in brain dopamine levels. However, these two groups did not show changes in glutamate levels compared to the SGL group. The TNF- $\alpha$  and NF $\kappa$ B levels in the brains were significantly elevated in the SGL control group versus the normal group. A dose-dependent decline in TNF- $\alpha$  levels was noticed in the naringin-treated groups (50 and 100 mg) (Figure 8C). However, NF $\kappa$ B was significantly reduced in the naringin (100 mg) group (Figure 8D).

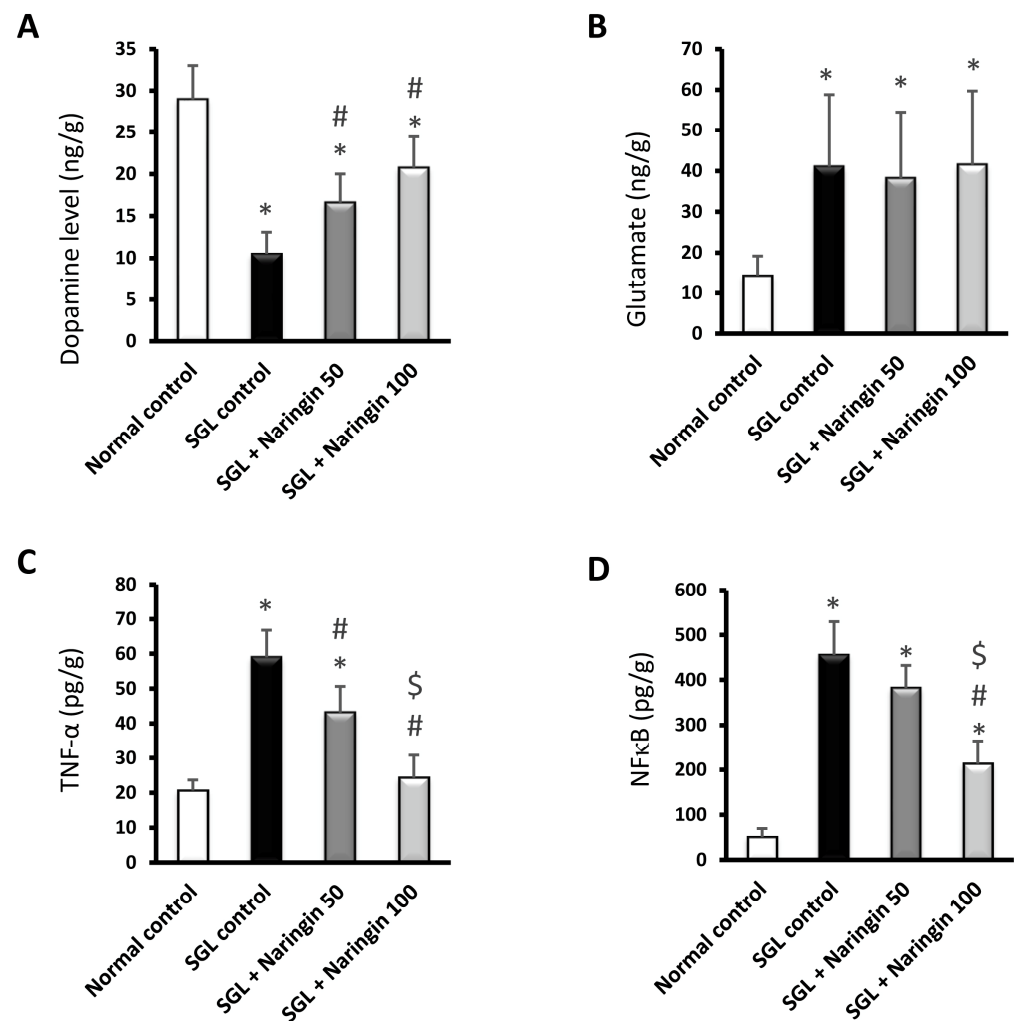


**Figure 8.** Naringin modulates the brain levels of glutamate, dopamine, and inflammation markers in mice fed with SGL. (A) Dopamine, (B) glutamate, (C) TNF- $\alpha$ , and (D) NF $\kappa$ B. Data are mean  $\pm$  SD. At  $p < 0.05$ , \* vs. normal, # vs. SGL control, and \$ vs. SGL + naringin-50.

### 2.3.4. RT-PCR Analysis

The results of the current study indicated a significant reduction in the expression of the Wnt gene and the  $\beta$ -catenin gene in the SGL mouse group. Conversely, the treatment with naringin at 50 mg and 100 mg resulted in upregulated genes. Additionally, the levels of the apoptotic genes, caspase-3 and BAX, were upregulated in the SGL mouse group and downregulated in both naringin-treated groups (50 and 100 mg). However, a significant difference was found in the expression level of the BAX gene between the naringin 50 mg and naringin 100 mg/kg groups. Moreover, the anti-apoptotic gene Bcl2 was downregulated in the SGL group compared with the normal group. Interestingly, treatment with naringin at both 50 mg/kg and 100 mg/kg caused the upregulation of Bcl2 expression levels, and this may suggest a protective effect of naringin against apoptotic events (Figure 9A–E).

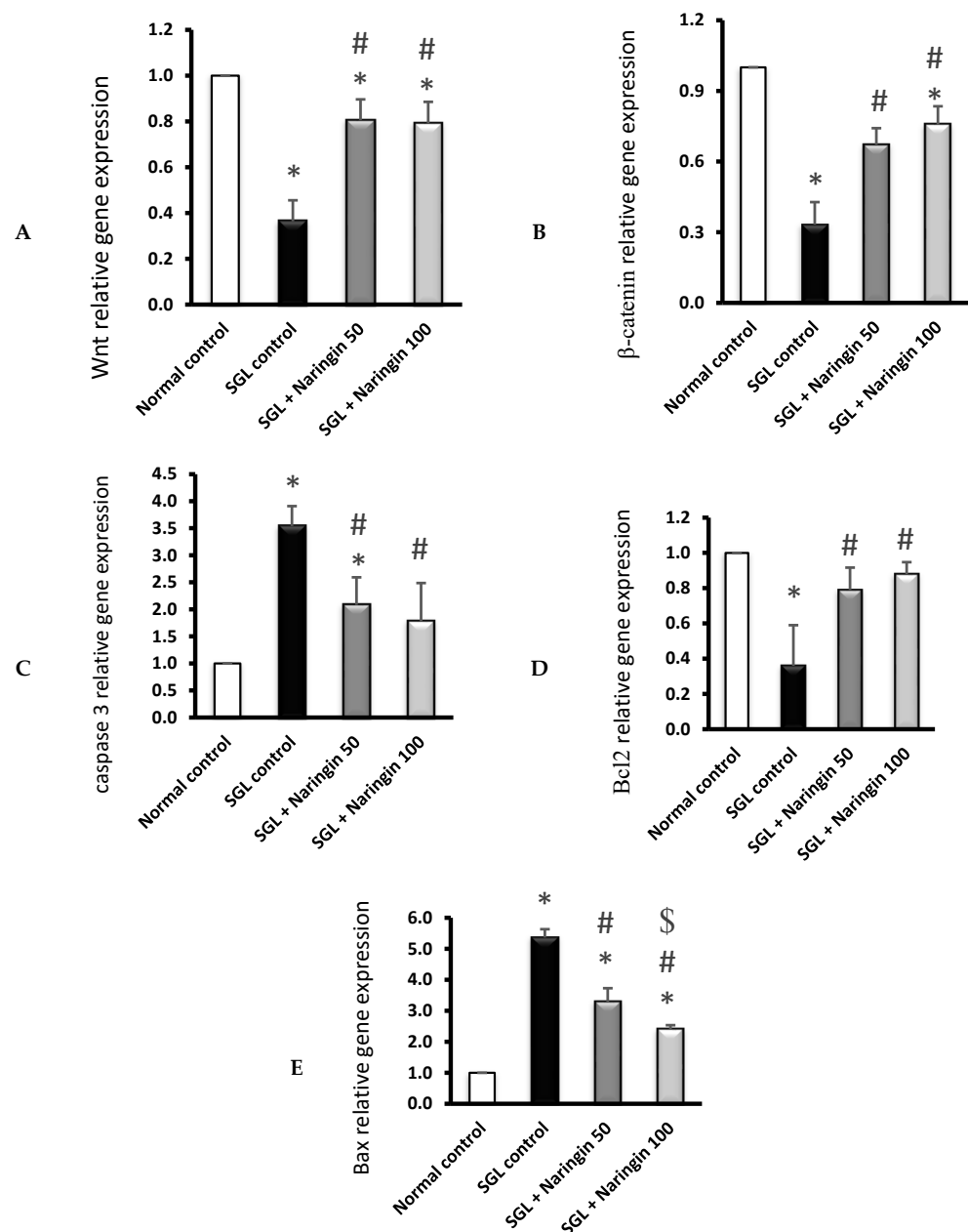


**Figure 9.** RT-PCR analysis of the expression of the target genes. (A) Wnt, (B)  $\beta$ -catenin, (C) caspase-3, (D) Bcl2, and (E) BAX. Data are means  $\pm$  SD, \* vs. normal control and # vs. SGL control, \$ vs. the SGL/naringin-50 group at  $p < 0.05$ .

### 2.3.5. Hematoxylin and Eosin Staining

In Figure 10, H&E-staining is demonstrated at sections in the hippocampus. The normal group shows neuron cell bodies arranged in a compacted form, and regular nuclei with intact fibrillary cytoplasmic processes are shown. The cortex shows normal neurons and astrocytic cells. The SGL control CA2 region shows smudged nuclei of neurons with pericellular vacuolation and mildly disrupted arrangement with decreased cellularity, and there are moderately disturbed fibrillary processes in multiple areas. The cortex shows degenerate neurons and increased vacuolation of astrocytic cells. In the SGL + naringin 50, the CA2 region shows focal pericellular vacuolation and scattered fibrillary process degeneration. The cortex shows mild degenerative changes to neurons and mild vacuolation of astrocytic cells (red arrow). The SGL + naringin 100 CA2 region shows a regular arrangement of neurons with cell bodies showing normal chromatin patterns and nuclei with minimal vacuolation (black arrow), and intact fibrillary processes. The cortex shows regular neurons with astrocytic cells showing minimal vacuolation.

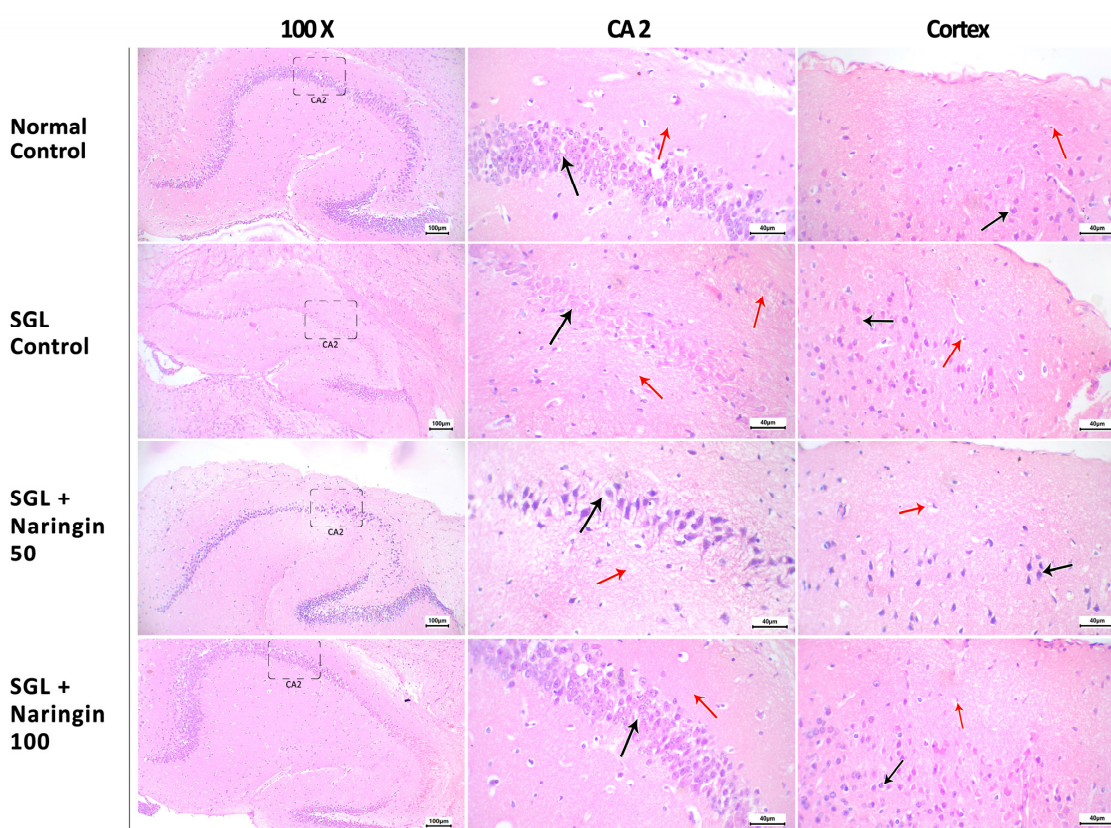


**Figure 10.** H&E-stained sections of the mice groups. The normal group shows neuron cell bodies arranged in a compacted form and regular nuclei, indicated by a black arrow, with intact fibrillary cytoplasmic processes (red arrow). The cortex shows normal neurons (black arrow) and astrocytic cells (red arrow). The SGL control CA2 region shows smudged nuclei of neurons with pericellular vacuolation and a mildly disrupted arrangement (black arrow) with decreased cellularity, and there are moderately disturbed fibrillary processes in multiple areas (red arrows). The cortex displays degenerate neurons (black arrow) and increased vacuolation of astrocytic cells (red arrow). The SGL + naringin 50 CA2 region shows focal pericellular vacuolation (black arrow) and scattered fibrillary process degeneration (red arrow). The cortex shows mild degenerative changes to neurons (black arrow) and mild vacuolation of astrocytic cells (red arrow). The SGL + naringin 100 CA2 region shows a regular arrangement of neurons with cell bodies showing normal chromatin patterns and nuclei with minimal vacuolation (black arrow), and intact fibrillary processes (red arrow). The cortex shows regular neurons (black arrow) with astrocytic cells showing minimal vacuolation (red arrow).

### 2.3.6. Immunohistochemical Staining for Bcl2

Figure 11 shows immunohistochemical staining in the hippocampi of the experimental groups. The normal control group showed organized neurons with strong cytoplasmic staining (first row). (However, the SGL control group showed less organized neurons with weak staining for Bcl2 (second row)). The SGL + naringin-50 group showed mild staining (third row), whereas the SGL + naringin-100 group showed moderate staining for Bcl2 (forth row).

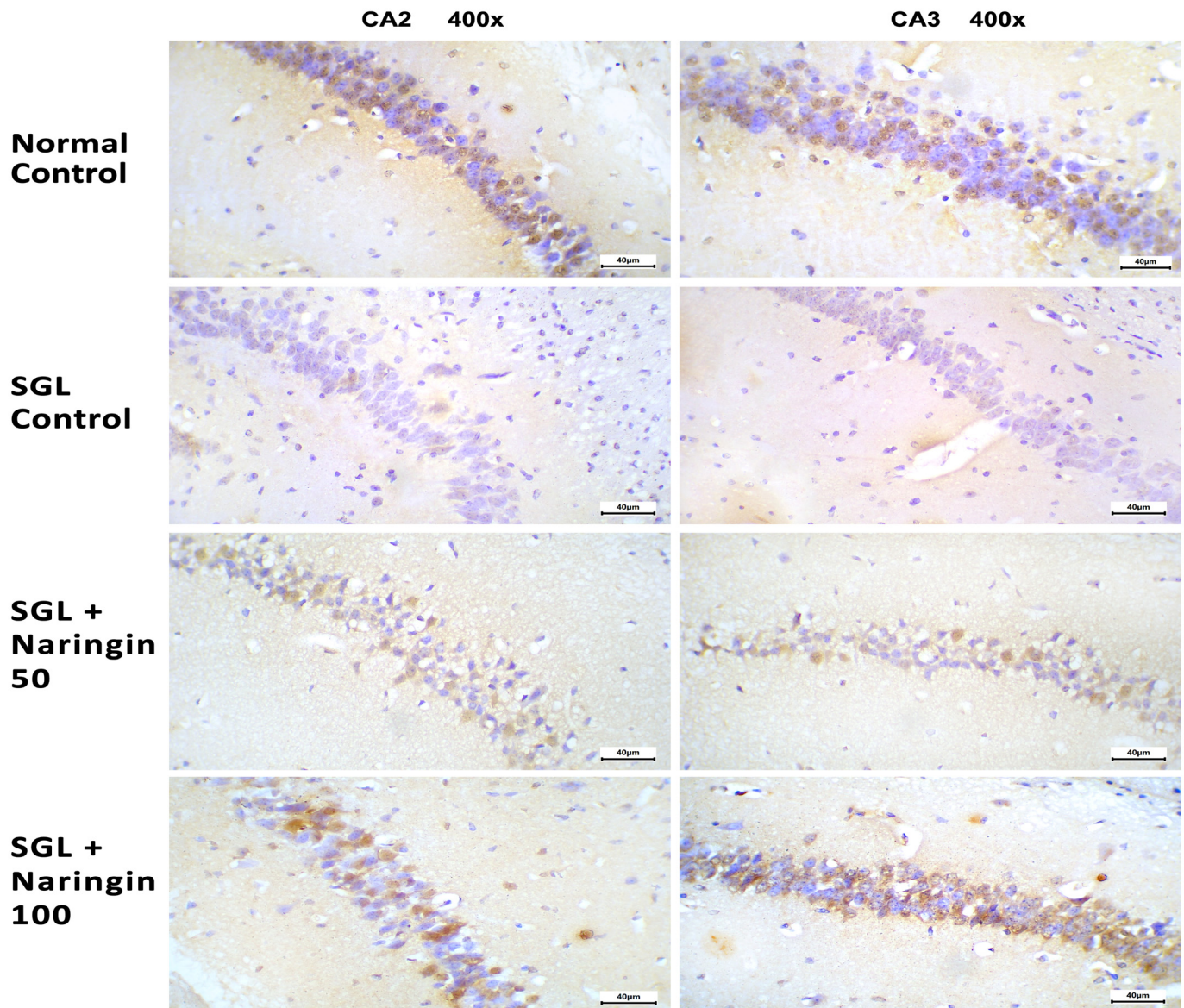


**Figure 11.** Immunohistochemical staining for Bcl2 in the hippocampi of the experimental groups. The normal group showed organized neurons with moderate-to-strong nuclear staining in most of the cells (CA2 and CA3 regions). The SGL control group showed less organized neurons with weak-to-absent staining for Bcl2 in most of the cells (CA2 and CA3 regions). The SGL + naringin-50 group showed mild-to-moderate staining in a few cells (CA2 and CA3 regions). The SGL + naringin-100 group showed improvements in the neuronal structures and moderate-to-strong staining for Bcl2 in most of the cells (CA2 and CA3 regions). Bcl2 immunostaining at  $\times 400$  magnification for both images in each group.

### 3. Discussion

ADHD is a neurodevelopmental disorder with onset in childhood. Failure to undergo treatment causes symptoms to worsen and complications to develop, including low self-esteem, school failures, depression, and addictions. In ADHD, non-pharmacological methods (directed at the child and their environment) and pharmacotherapy are used. However, at present, pharmacotherapy for this disorder is not effective enough, and new, more effective methods of therapy are still being sought. In the presented manuscript, the authors used bioinformatic and behavioral studies for evaluating the effect of naringin in the ADHD model and the mechanism of the presented results.

In the molecular docking study, a careful literature review showed that naringin could bind to several targets, as suggested by molecular modeling and demonstrated experimentally. These biological targets include HSP90, P53, IL-6, STAT3, ESR1, BCL-2, GSK-3 $\beta$ , CASP3, and MMP2. Among these proteins, HSP90 and GSK-3 $\beta$  could be implicated in the activation of the Wnt/ $\beta$ -catenin signaling pathway, as previously reported [18,48]. To understand the molecular basis of the interaction of naringin with these targets, a molecular docking simulation of naringin was conducted with HSP90 and GSK-3 $\beta$ . The simulation showed a satisfactory binding with GSK-3 $\beta$ , including the critical interaction with the kinase hinge region. Many glycosides could have the ability to interact with the hinge region residues of GSK-3 $\beta$ , using their sugar part in a similar manner to naringin. Nevertheless, what makes naringin unique is its naringenin aglycone part, which has interesting complementarity with the hydrophobic back pocket of GSK-3 $\beta$  and can form an extensive network of H-bonds with its polar residues. Next, we turned our attention to investigating the potential interaction of naringin with HSP90, which is an ATP-dependent molecular chaperone that plays a key role in folding various client proteins [49]. It was obvious from the proposed docking pose that the disaccharide fragment has the perfect size for filling the polar pocket, making H-bonds with the critical Asp93 and Thr184, which similarly interact with ATP and the inhibitor JMC31. In addition, the chromene ring largely contributed to the binding via its  $\pi$ -stacking and hydrophobic interactions with Phe138 and Leu107, respectively. The above observations suggest the potential implication of these biological targets in the activation of Wnt/ $\beta$ -catenin signaling by naringin and may provide guidelines for the discovery of other bioactive glycosides with a similar mode of action.

Notably, previous studies proposed the binding of naringin into the ATP pocket of these enzymes, with the sugar moieties anchored to the critical polar residues responsible for stabilizing the ATP polar part [50,51]. The MD simulation provided more confidence in the proposed binding modes of naringin to both targets. We believe that the stable H-bonding interactions with Lys85 and Lys183 are responsible for the selectivity of naringin for GSK-3 $\beta$  over other kinases. Similarly, the simulation study showed that the anchoring of the sugar moiety to the critical Asp93 and Thr184 helps to stabilize the ligand in the ATP site of HSP90. These findings could encourage the search for similar flavonoids or the design of naringin derivatives to target GSK-3 $\beta$  and HSP90 for a variety of therapeutic applications.

These results were supported by a previously published study on the docking of naringin on GSK-3 $\beta$  (PDB ID: 1Q4L) using AutoDock tools, which also demonstrated the H-bond between disaccharide and Val135, in addition to the H-bond between the aglycon part and Lys 85 [52].

In our study, the bioinformatic analysis of the naringin mechanism of action was represented in the canonical Wnt signaling pathway using the KEGG database. Wnt proteins are produced and bind to their ligands, which causes stabilization of the cytoplasmic  $\beta$ -catenin. The  $\beta$ -catenin is subsequently allowed to move to the nucleus and stimulate the Wnt-regulated genes via interacting with the transcription factors and coactivators. Upon analyzing the interaction between the studied proteins using the STRING database, a network was produced with nodes representing proteins and colored edges representing different types of interactions between the proteins. The interactions include text-mining, gene co-occurrence, gene homology, interactions from curated databases, and experimentally determined interactions. The bioinformatic enrichment analysis of naringin target

genes has shown a strong relation between a relatively large number of target genes and cognitive disorders like Parkinson's disease and Alzheimer's disease, which could indicate a relationship with other cognitive disorders, such as ADHD. Many studies support us by demonstrating that the canonical Wnt/ $\beta$ -catenin signaling pathway is active in the cortex during embryogenesis [53–55], and it controls the time and duration of neurogenesis [54,56].

The analysis and visualization of naringin and ADHD target genes and pathways showed that 13 pathways are common between the drug and the disease, which may support the relationship between naringin and ADHD. The findings of Ishii et al. suggest that naringin may facilitate the recovery of dopaminergic neurons after injury by restoring growth differentiation and neurotrophic factor (GDNF) levels in the substantia nigra and reducing Iba-1 and TNF- $\alpha$  levels in the striatum [57].

In the current study, behavioral parameters validated the use of SGL as a tool to induce ADHD-like symptoms in mice. The SGL group showed a significant prolongation of the grooming time in the self-grooming test, and a low percentage of mice succeeded in crawling with the rope. Furthermore, the ASST showed an increased number of required trials for the CD, RV1, and IDS criteria, implying that poor attention was noticeable in the mice fed on SGL. Similar to our results, Heisler et al. reported that animals with deficits in cognitive flexibility denoted by defective performance in the ASST need more trials to perform the tasks in the ASST [58].

Previous studies documented that oral naringin has effect on locomotion, attention, or learning capabilities per se. For example, Swamy et al. tested oral naringin 100 mg/kg in the open field test, novel object recognition test, and forced swimming test, and claimed it was inert and did not affect motor activity or cognitive function [59]. Another study, performed by Dai et al., tested the effect of oral naringin in rats in the Morris water maze, novel object recognition, and fear condition test; the authors concluded that no significant effects were observed in the animals treated with naringin 100 mg/kg [60].

The current results indicate high brain glutamate levels in the brains of mice fed with SGL. Increments in glutamatergic transmission in brain regions such as the frontal, striatal brain, and anterior cingulate cortex are linked to ADHD [61,62]. Glutamate upregulation is observed in ADHD models and other neurologic disorders [63,64]. In agreement with our study, previous rodent models of ADHD demonstrated increased brain glutamate levels in rats [33,65,66] and mice [32].

In contrast to glutamate, dopamine was found to decline in the brains of the mice fed on SGL. Similar results were obtained in animal models of ADHD based on SGL diets [32,33,66]. Dopamine deficiency is known to play a critical role in the pathology of ADHD. Imaging studies have provided additional supportive evidence of the possible involvement of catecholamine and neurotransmitter dysregulations in the etiology of ADHD. Functional imaging studies, such as positron emission tomography, which utilize selective ligands for the dopamine transporter (DAT), documented amplified DAT binding capacity in up to 70% of ADHD patients, designating a greater density of DAT in the ADHD brains than in controls [5,6]. In agreement with this, altered D2/D3 receptor availability that is responsive to methylphenidate was reported in ADHD patients [67,68]. Medications used for ADHD treatment, e.g., methylphenidate, amphetamines, and bupropion, act by inhibiting the reuptake of dopamine [69–71]. Furthermore, ADHD is linked to a decline in the availability of noradrenaline transporters in frontoparietal–thalamic–cerebellar regions [7]. In ADHD patients, the lack of appropriate performance in attention tasks correlates with low concentrations of urinary excreted noradrenaline metabolites [72].

In the current study, there was a reduced expression of brain Wnt/ $\beta$ -catenin genes and Bcl2, but overexpression of caspase 3 and BAX, in the mice fed with SGL. One study examining adult ADHD found that the KCNIP4 gene was associated with ADHD. This gene is part of a negative feedback loop within the Wnt/ $\beta$ -catenin pathway [73]. A connection between Wnt signaling and mental disorders was documented [74]. The Wnt signaling pathways are activated by the joining of Wnt-protein ligands to the cell-surface receptors, which are referred to as Frizzled, followed by the recruitment of Dishevelled (DVL) proteins.

Indeed, the Wnt/ $\beta$ -catenin signaling pathway controls cell death and survival [75]. Some studies revealed a correlation between Wnt/ $\beta$ -catenin activation and the triggering of apoptosis, involving the overexpression of BAX and caspases-3, and the downregulation of Bcl2 [76].

The Wnt pathway contributes to Alzheimer's disease. In brief, amyloid- $\beta$  (A $\beta$ ) neurotoxicity in Alzheimer's disease leads to downregulated Wnt signaling [77], which suggests that downregulated Wnt may be crucial in Alzheimer's pathogenesis. Similarly, Ye et al. highlighted suppressed downstream canonical Wnt signals in senescent human cells [78] and reported that downregulated Wnt signaling stimulates senescence-linked heterochromatin focus.

Importantly, Wnt/LRP6 signaling is crucial for the regulation of axon remodeling, synaptic plasticity, and  $\beta$ -catenin-independent neurotransmitter release [79]. Grünblatt et al. (2018) reported activation of the Wnt/ $\beta$ -catenin pathway and the improvement of neuronal differentiation through treatment with methylphenidate [23]. This work shed light on the additional targets of methylphenidate and ADHD candidates. Custodio et al. provided evidence that Wnt signaling is involved in the behavioral impairment in the thyroid-hormone-responsive protein-overexpressing ADHD mouse model [22]. Caracci et al. concluded that activation of Wnt/ $\beta$ -catenin signaling is influential in developing new therapeutic options that may help support ADHD patients [80]. In agreement with Caracci et al., another research group concluded that the Wnt/ $\beta$ -catenin pathway is disrupted in patient-specific neural stem cells [25].

The anti-inflammatory and anti-apoptotic effects of naringenin led to the assumption that it is promising for treating neurodegenerative disorders [81]. Naringenin was found to improve spatial learning and memory deficiency in the AD model; this effect was thought to be mediated through regulation of the PI3K/AKT/GSK-3 $\beta$  pathway and downregulation of Tau phosphorylation [82]. Further, naringenin was proven to affect apoptosis and prevent neurotoxicity. The mechanisms by which naringenin performs anti-apoptotic activity and exerts neuroprotective effects involve caspase-3-pathway inhibition, PI3K/AKT activation, and GSK-3 $\beta$  signaling pathway modulation [83]. Moreover, naringenin inhibits lipid peroxidation by decreasing the content of malondialdehyde in the hippocampal brain [84].

The exact mechanism of action of naringenin is still to be investigated. The activities of flavonoids rely on their antioxidant and metal-chelating actions [85,86]. As the chemical structure belongs to polyphenols, flavonoids are exceptional free radical scavengers as a result of the high reactivity of their hydroxyl substituents. This free-radical-scavenging activity occurs in addition to the chelating properties of flavonoids, mediated the repressive effect of flavonoids on lipid oxidation. One study highlighted the ability of naringin to scavenge free radicals and lipid peroxides [87]. Further, naringin was described as a protectant against DNA cleavage [88]. In animal models, mice were treated with naringin prior to exposure to multiple grades of  $\gamma$ -radiation [36]. In addition, naringin was documented to mitigate ifosfamide-induced micronuclei in mouse bone marrow [89]. The impact of naringin on Wnt signaling has been reported in some other disorders. One of the studies on this topic investigated the probable role of Wnt/GSK-3 $\beta$ / $\beta$ -catenin signaling in hyperthyroidism-induced disorders and explored the beneficial actions of orally administered naringin for 2 weeks in rats with hyperthyroidism via influencing the expression of Wnt/ $\beta$ -catenin proteins [90].

Bcl2 is an antiapoptotic factor that acts by preventing BAX, which promotes the apoptosis of nucleus pulposus cells. Naringin at 20  $\mu$ g/mL noticeably enhanced the production of Bcl2 and mitigated BAX expressions. In turn, the results revealed in this study explained how naringin was effective in suppressing apoptosis via the mitochondrial pathway [91]. This finding explains the results of the current study; an increase in gene production of Bcl2 was noticed upon treating mice with naringin 50 mg/kg and 100 mg/kg. Furthermore, decreases in Wnt,  $\beta$ -catenin, caspase 3, and BAX mRNA expressions were observed.



## 4. Materials and Methods

### 4.1. Investigation by Molecular Docking and Molecular Dynamic Simulation

#### 4.1.1. Molecular Docking

To understand the binding mode of naringin to its targets, we docked the compound into the X-ray crystal structures of GSK-3 $\beta$  (PDB ID: 4AFJ) and HSP90 (PDB ID: 8AGI), obtained from the protein databank ([www.rcsb.org](http://www.rcsb.org), accessed on 1 September 2024).

Molecular docking was performed using the FRED module implemented in OpenEye software 2023.2.3 and the Fast Rigid Exhaustive Docking method. The first step was the generation of a conformer library of naringin using the Omega module and the default settings. Next, a design unit, which comprised the prepared receptor grids, was generated using the make-receptor graphical interface provided in the OpenEye suite. The docking box was centered on the atoms of the crystallized ligands in both cases. Finally, the software performed rigid docking using the multi-conformer ligand library [92]. The 1.98 Å crystal structure of GSK-3 $\beta$  in complex with an oxazole inhibitor (PDB ID: 4AFJ) and the 2.10 Å crystal structure of HSP90 in complex with JMC31 (PDB ID: 8AGI) were used for docking simulation. The default scoring function of the FRED module is the Chemgauss4 function, which depends on shape complementarity. Eight types of interactions are included in the score, namely, steric, acceptor, donors, coordinating groups, metals, lone pairs, polar hydrogens, and chelator coordinating groups. Docking poses with the best scores were visually examined and the graphics were rendered using Pymol 2.5.5.

#### 4.1.2. Molecular Dynamic Simulation

Subsequently, docked poses with the best scores were further examined in complex with each enzyme through a 100-nanosecond MD simulation to gain insights into their binding determinants. Using the Desmond module in Schrodinger software (Version 2020.1), the naringin in complex with GSK-3 $\beta$  and HSP90 was separately solvated by a truncated octahedral box of TIP3P waters with a 12 Å distance between the farthest dimensions of the complex in each direction. The numbers of atoms were 47,508 and 29,615 in the GSK-3 $\beta$  and HSP90 systems, respectively. Each system was then minimized for 300 ps using the default parameters and simulated in an NPT ensemble and Nosé–Hoover thermostat for 100 ns and with a 2 fs timestep, with frames recorded every 10 ps. The trajectories were analyzed using the simulation interaction diagram within the Schrodinger software and visualized using Pymol software.

### 4.2. The Utilization of Bioinformatic Tools to Correlate the Target Proteins

A search on the KEGG database [93] was performed for exploring the mechanism of naringin and how it may affect the targeted pathway (on 3 July 2024). The input was as follows: Wnt,  $\beta$ -catenin, caspase 3, Bcl2, and BAX. Proteins with possible interactions with Wnt/ $\beta$ -catenin were studied and enriched by searching gene ontology, and pathway analysis was performed with the demonstration of the co-expressed proteins and their scores through using the String database, last accessed 20 September 2024 using the following link: (<https://string-db.org/>, accessed on 1 September 2024).

On 5 July 2024, the binding database was used to explore naringin targets with 0.7 similarity. Next, the naringin target genes were entered into the KEGG mapper to check the related pathways. On 8 July 2024, ADHD-related genes were retrieved from the DisGenet database using a GDA score of more than 0.4. Furthermore, naringin target genes were introduced in the ShinyGo 0.80 bioinformatic tool to make an enrichment analysis with an FDR cutoff of 0.05 on 11 July 2024 to look for a relation between the drug and the disease.

On 18 July 2024, we utilized the FunRich 3.1.3 bioinformatic tool for visualization and analysis of target genes and pathways. In addition, a Venn diagram was created for the shared pathways between naringin and ADHD. In addition, a network of the naringin target genes and pathways from one side and ADHD from another side was created using Cytoscape 3\_10\_2 on 19 July 2024.

### 4.3. The Mouse In Vivo Study

#### 4.3.1. Chemical Preparation

Monosodium glutamate (SGL) was procured from Algomhoria Company (Cairo, Egypt) and included in a fixed portion mixed with a standard diet (0.4 g/kg). Naringin (C<sub>27</sub>H<sub>32</sub>O<sub>14</sub>) was obtained as a white powder from Alfa Aesar (ThermoFisher Company, GmbH, Dreieich, Germany), prepared as a suspension in 1% CMC aqueous solution in distilled water, and given to mice by an oral gavage tube.

#### 4.3.2. Mouse Environment and Housing Conditions

Male Swiss albino mice (3 to 4 weeks old, with a body weight range of 9–15 g) were kept in polyethylene cages in groups of six mice. Mice were maintained in the animal facility at Suez Canal University. A normal D/L cycle was maintained (13 h for the lighting phase and 11 h for the dark phase at that time of the year). Free access to the prepared food mixture and clean tap water were provided to the mice throughout the experiment. The experimental procedures received approval from the Medicine Ethical Committee at Suez Canal University (5690#).

#### 4.3.3. Experimental Design

The male Swiss albino mice were divided equally and randomly into four experimental groups with different dietary compositions and drug treatments, as shown in Table 1. The normal chow diet given to Group 1 was composed mainly of crushed yellow corn, whereas the SGL diet was composed of the same normal chow diet—like that administered to Group 1—but mixed with 0.4 g of SGL for every 1 kg of normal diet.

**Table 1.** The experimental groups in the mouse study.

Number	Name	Applied Diet	Treatment
Group 1	Normal control	Normal chow diet *	Distilled water
Group 2	SGL control	SGL diet † [94]	Distilled water
Group 3	SGL + naringin-50 mg/kg	SGL diet	Naringin 50 mg/kg [95]
Group 4	SGL + naringin-100 mg/kg	SGL diet	Naringin 100 mg/kg [59,60]

\* The normal chow diet was composed mainly of crushed yellow corn. † The SGL diet was composed of SGL (0.4 g/kg) for each 1 kg of the normal chow diet [94].

#### 4.3.4. Evaluation of Mouse Psychomotor Activity by Behavior Tasks

##### Self-Grooming Test

The mice were observed for impulsive grooming activities, such as face rubbing and licking or biting paws and fur, following a previous report [96], with some modifications. Each mouse was placed into a cage with dimensions equal to 38 cm × 25 cm × 23 cm for an assessment period of 10 min [97].

##### Rope Crawling Test

During this test, each mouse was suspended for three minutes on a 2 m long rope positioned 150 cm above the floor of the room (altitude stress) and observed for their responses. The quantification of mice that were able to grab or crawl down the hung rope in a “successful” manner was performed, but the mice that were unable to crawl up the rope or grasp it securely were considered to have “failed” this test. Both criteria were quantified. The success rate of each experimental group was calculated for statistical analysis [98].

##### Attentional Set-Shifting Task (ASST)

The ASST was performed following a previously published protocol [99]. The testing arena was rectangular and made of plexiglass with the following dimensions, 40 × 80 × 30 cm. The task contained 2 transferable plates dividing the arena into equal thirds (by length). The first third, on the left side, was considered the starting box, and there was a removable

panel placed in the right third to divide it into two equal sections; each section had a pot (Figure 12).

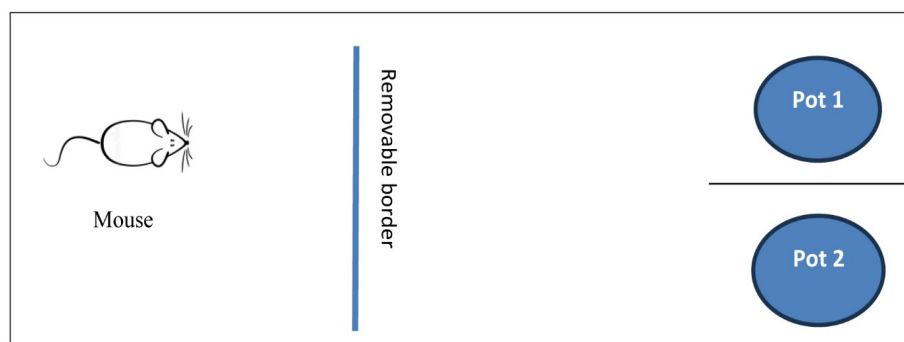


**Figure 12.** A diagram of the attention set-shifting task (ASST) for mice.

- The Habituation Phase (5 Days)

Each mouse was trained for 20 min/day to freely explore the arena without any testing stimuli for 5 days (with a restricted fixed basal diet not leading to loss of more than 15% of their body weight). A food reward (which was a piece of cereal) was introduced to the cage to make it familiar to the mouse (regarding color and odor).

- The Training Phase (2 Days)

Training was performed on days 6 and 7 (2 training days). To obtain a food reward in the pot (without filling), 3 successful attempts were required. The mouse was trained on digging in the pots media to obtain the food reward embedded in cage bedding.

Mice were empowered to detect the presence/absence of the food reward (cereal) in the pot by either an olfactory stimulus (odor related to the digging medium) or a tactile stimulus (texture of the digging medium). The training was achieved by enabling the mice to dig for the food reward until finishing 6 consecutive correct trials with the accurate choice for the pot. Animals that failed to dig for food rewards within 2 h from the start of training were excluded. The examples used in training were not used again for testing.

- Experimentation Phase (1 Day)

On day 8 (the experimentation day), the first step in training was simple discrimination (SD) between the pots, which were different in one aspect (either an olfactory stimulus or a tactile stimulus). After completing the required training, the mice were shifted to another test for compound discrimination (CD), in which the familiar pots were used in the SD with a similar reward aspect, but after introducing a second, non-relevant aspect.

After the mice learned the assigned training idea, the reinforcement rules were revised, and the mice were trained to identify that the originally exact stimulus within the rewarded aspect had become “not correct” during this phase; this stage was designated as reversal-1 (RV1). After mice accomplished the criterion for RV1, they were moved to a new testing idea. Intra-dimensional shift (IDS) was achieved by presenting the mice with a new group of stimuli, but they were commanded to pay attention to the same perceptual aspect reinforced during the SD, CD, and RV1. The test was completed at the start of the dark phase of the day (5–7 pm).

In summary, a 3 min trial was allowed to determine each mouse choice. In the waiting area, mice had free access to water to offer a chance to drink and prevent thirst. In the experimentation phase, the total number of trials made by each mouse for reaching the criterion set with each stage was registered and compared.

#### 4.3.5. Mouse Scarification

The mice received an injection of ketamine (85 mg/kg) [100] and were then sacrificed by cervical dislocation. Next, the brains were dissected, blood was washed out, and

the brains divided into 2 separate hemispheres. The right hemisphere was fixed in 4% paraformaldehyde solution to be used later for histological staining [100], and the left brain hemisphere was subjected to immediate freezing at  $-80^{\circ}\text{C}$ .

#### 4.3.6. Molecular Analysis

Homogenized brain tissues (15 mg) were used to extract total RNA. This was performed using the miRNeasy mini kit purchased from QIAGEN (CAT. NO.217004, Hilden, Germany). Next, complementary DNA was obtained after converting RNA to cDNA utilizing QuantiTect Reverse Transcription Kit obtained from QIAGEN company (CAT. NO.205311, Germany). Finally, gene analysis for Wnt,  $\beta$ -catenin, caspase-3, Bcl2, and BAX was computed in StepOne real-time PCR instrument from Thermo Scientific Company (CAT. NO. 4376357, Oxford, UK). The reaction volume included 10  $\mu\text{L}$  of HERA SYBR<sup>®</sup> Green qPCR master mix (Willowfort, Birmingham, UK) and 15 pmol from primer pairs, as shown in Table 2, and 150 ng of cDNA, and the conditions used were initial denaturants at  $95^{\circ}\text{C}$  for 5 min session, followed by 40 cycles of denaturant  $95^{\circ}\text{C}$  for half a minute, annealing at  $58\text{--}60^{\circ}\text{C}$  for the 30 s, and extension at  $72^{\circ}\text{C}$  for 30 s. The mRNA fold changes for the target genes were determined by applying the  $2^{-\Delta\Delta\text{Ct}}$  method [101], and normalized gene expression was achieved relative to the  $\beta$ -actin gene.

**Table 2.** Primer sequences for target genes.

GenesPrimers	Sequences	Accession Number
<i>Wnt</i>	Forward 5'/GCCTGTGAAGGACTCAGAACTTG3' Reverse 5'/AGCTGTCACTGCCGTTGGAAGT3'	NM_001285794.1
$\beta$ -Catenin	Forward 5'/GTTCGCCTTCATTATGGACTGCC3' Reverse 5'/ATAGCACCTGTTCCTCCGCAAAG3'	NM_007614.3
<i>Caspase-3</i>	Forward 5'/GGAGTCTGACTGGAAAGCCGAA3' Reverse 5'/CTTCTGGCAAGCCATCTCCTCA3'	NM_009810.3
<i>Bcl2</i>	Forward 5'/CCTGTGGATGACTGAGTACCTG 3' Reverse 5'/AGCCAGGAGAAATCAAACAGAGG3'	NM_009741.3
<i>BAX</i>	Forward 5'/AGGATGCGTCCACCAAGAAGCT3' Reverse 5'/TCCGTGTCCACGTCAGCAATCA3'	NM_007527.3
$\beta$ -actin	Forward 5'/TCCTCCTGAGCGCAAGTACTCT3' Reverse 5'/GCTCAGTAACAGTCCGCCTAGAA3'	NM_007393.5

#### 4.3.7. Assessment of Inflammatory Mediators

Brain tissues were homogenized in RIPA buffer (Sigma-Aldrich Chemie GmbH, Buchs, Switzerland) and homogenates were cleared via centrifuging at  $1500\times g$ . ELISA kits for dopamine (Catalog # MBS732020), glutamate (Catalog # MBS756400nd), TNF- $\alpha$  (Catalog # MBS825075), and NF $\kappa$ B (Catalog # MBS043224) were used in this study. The kits were purchased from MBS Company (San Diego, CA, USA) and the measurement of the reaction products was performed at 450 nm.

#### 4.3.8. Histopathology, Immunohistochemical Staining, and Examination

The right hemispheres were formalin-fixed, and then implanted in liquid paraffin, and were allowed to cool. Sections (4  $\mu\text{m}$  in thickness) were prepared from the paraffin blocks. For routine examination, sections were cut and stained with hematoxylin and eosin to show the neuron cell body arrangement and the appearance of the nuclei and the fibrillary cytoplasmic processes [64,102].

Other sections were allowed to dry and then subjected to immunohistochemical staining for Bcl2 using rabbit polyclonal antibodies (cat # A16776, ABclonal, Swansea, UK). Next, the horseradish peroxidase label was applied for 1 h, followed by DAB chromogen for 14 min using the Mouse/Rabbit PolyDetector detection system (Cat# BSB0205, Bio

SB, Goleta, CA, USA). Mayer's hematoxylin was utilized to counterstain the tissues. All slides were imaged at 400×, using the Leica Microsystems. A calibrated standard digital microscope camera was fixed to a Leica microscope (Leica model DM 1000, Heidelberg, Germany), with 10 megapixel resolution (3656 × 2740 pixels). Morphometric comparison for the color area in each section was set [103] for Bcl2 in the hippocampus by alienating the area stained with DAB from hematoxylin and converting the color information to red, green, and blue (RGB) images with multiple stains [104].

#### 4.3.9. Statistical Analysis and Data Manipulation

Data were collected by the authors, tabulated, and then presented as the mean and standard deviation. Comparison between groups was achieved by application of the one-way ANOVA test and Bonferroni's test at  $p < 0.05$  considering all possible comparisons among the study groups. Quantal data were analyzed using the Chi-squared test.

## 5. Conclusions

In conclusion, the bioinformatic study indicated that Wnt/ $\beta$ -catenin is involved in the naringin mechanism of action; this is a common pathway in neurologic disorders. Furthermore, molecular docking indicated the possible inhibition of GSK-3 $\beta$  and HSP90 by naringin.

The mouse study highlighted that feeding mice with SGL for eight weeks produced behavioral signs of ADHD in these mice; poor attention was observed in the ASST and rope crawling test, and locomotor hyperactivity was observed in the grooming test. The brains showed downregulated levels of Wnt/ $\beta$ -catenin and Bcl2 proteins and upregulated inflammatory mediators. In mice cotreated with naringin, the behavioral signs of ADHD were diminished, and the inflammatory markers were downregulated. In addition, upregulation of Wnt/ $\beta$ -catenin and Bcl2 proteins and downregulation of caspase 3 and BAX were observed. These results open avenues for more studies on the role of naringin in ADHD models to fully elucidate its mechanism of action.

**Author Contributions:** Conceptualization, S.A.Z. and N.M.A.E.-F.; Data curation, K.E.-S. and M.K.E.-K.; Formal analysis, H.I.M., N.A., S.M.M.M. and A.A.A.; Investigation, S.A.Z., R.M.L., N.A., S.A.S., M.A.H., M.K.E.-K., M.S.F. and N.M.A.E.-F.; Methodology, H.I.M., S.A.Z., K.E.-S., R.M.L., M.K.E.-K., N.M.A.E.-F. and N.A.; Resources, R.M.L., N.A. and A.A.A.; Software, H.I.M., S.M.M.M., S.A.S., M.A.H., M.K.E.-K., M.S.F. and N.M.A.E.-F.; Validation, K.E.-S., R.M.L., S.M.M.M. and M.S.F.; Visualization, S.M.M.M., S.A.S., A.A.A. and M.A.H.; Writing—original draft, H.I.M., S.A.Z., K.E.-S., S.M.M.M., M.A.H., M.K.E.-K., M.S.F., N.M.A.E.-F. and K.E.-S.; Writing—review and editing, H.I.M., S.A.Z., R.M.L., N.A., S.A.S. and A.A.A. All authors will be informed about each step of manuscript processing, including submission, revision, revision reminder, etc., via emails from our system or the assigned Assistant Editor. All authors have read and agreed to the published version of the manuscript.

**Funding:** The authors extend their appreciation to the King Salman Center for Disability Research for funding this work through Research Group no. KSRG-2023-104.

**Institutional Review Board Statement:** The animal study protocol was approved by the Ethics Committee at the Faculty of Medicine in Suez Canal University (protocol code 5690# and date of approval 27 May 2024).

**Informed Consent Statement:** Not applicable.

**Data Availability Statement:** The original contributions presented in this study are included in the article. Further inquiries can be directed to the corresponding author.

**Conflicts of Interest:** The authors declare no conflicts of interest.

## References

- Song, P.; Zha, M.; Yang, Q.; Zhang, Y.; Li, X.; Rudan, I. The Prevalence of Adult Attention-Deficit Hyperactivity Disorder: A Global Systematic Review and Meta-Analysis. *J. Glob. Health* **2021**, *11*, 4009. [[CrossRef](#)] [[PubMed](#)]
- Vasiliadis, H.-M.; Lunghi, C.; Rahme, E.; Rochette, L.; Gignac, M.; Massamba, V.; Diallo, F.B.; Fansi, A.; Cortese, S.; Lesage, A. ADHD Medications Use and Risk of Mortality and Unintentional Injuries: A Population-Based Cohort Study. *Transl. Psychiatry* **2024**, *14*, 128. [[CrossRef](#)] [[PubMed](#)]
- Sharma, A.; Couture, J. A Review of the Pathophysiology, Etiology, and Treatment of Attention-Deficit Hyperactivity Disorder (ADHD). *Ann. Pharmacother.* **2014**, *48*, 209–225. [[CrossRef](#)] [[PubMed](#)]
- Giannopoulou, I.; Pagida, M.A.; Briana, D.D.; Panayotacopoulou, M.T. Perinatal Hypoxia as a Risk Factor for Psychopathology Later in Life: The Role of Dopamine and Neurotrophins. *Hormones* **2018**, *17*, 25–32. [[CrossRef](#)] [[PubMed](#)]
- Soliva, J.C. Neuroimaging in the Diagnosis of ADHD: Where We Are and Where We Are Going. *Expert Opin. Med. Diagn.* **2011**, *5*, 307–318. [[CrossRef](#)]
- Minzenberg, M.J. Pharmacotherapy for Attention-Deficit/Hyperactivity Disorder: From Cells to Circuits. *Neurotherapeutics* **2012**, *9*, 610–621. [[CrossRef](#)]
- Rosa-Neto, P.; Lou, H.C.; Cumming, P.; Pryds, O.; Karrebaek, H.; Lunding, J.; Gjedde, A. Methylphenidate-Evoked Changes in Striatal Dopamine Correlate with Inattention and Impulsivity in Adolescents with Attention Deficit Hyperactivity Disorder. *NeuroImage* **2005**, *25*, 868–876. [[CrossRef](#)]
- Sun, H.; Wu, M.; Wang, M.; Zhang, X.; Zhu, J. The Regulatory Role of Endoplasmic Reticulum Chaperone Proteins in Neurodevelopment. *Front. Neurosci.* **2022**, *16*, 1032607. [[CrossRef](#)]
- Chang, P.-K.; Chu, J.; Tsai, Y.-T.; Lai, Y.-H.; Chen, J.-C. Dopamine D3 Receptor and GSK3 $\beta$  Signaling Mediate Deficits in Novel Object Recognition Memory within Dopamine Transporter Knockdown Mice. *J. Biomed. Sci.* **2020**, *27*, 16. [[CrossRef](#)]
- Fu, C.; Lei, Y.; Liang, L.; Jiang, J.; Qin, Y.; Lao, Y.; Tan, Z.; Wang, Y.; Liu, Q. Characterization of HSP90 Expression and Function Following CNS Injury. *Neurosci. Lett.* **2024**, *836*, 137875. [[CrossRef](#)]
- McFarland, N.R.; Dimant, H.; Kibuuka, L.; Ebrahimi-Fakhari, D.; Desjardins, C.A.; Danzer, K.M.; Danzer, M.; Fan, Z.; Schwarzschild, M.A.; Hirst, W.; et al. Chronic Treatment with Novel Small Molecule Hsp90 Inhibitors Rescues Striatal Dopamine Levels but Not  $\alpha$ -Synuclein-Induced Neuronal Cell Loss. *PLoS ONE* **2014**, *9*, e86048. [[CrossRef](#)] [[PubMed](#)]
- Putchá, P.; Danzer, K.M.; Kranich, L.R.; Scott, A.; Silinski, M.; Mabbett, S.; Hicks, C.D.; Veal, J.M.; Steed, P.M.; Hyman, B.T.; et al. Brain-Permeable Small-Molecule Inhibitors of Hsp90 Prevent  $\alpha$ -Synuclein Oligomer Formation and Rescue  $\alpha$ -Synuclein-Induced Toxicity. *J. Pharmacol. Exp. Ther.* **2010**, *332*, 849–857. [[CrossRef](#)] [[PubMed](#)]
- Wang, B.; Liu, Y.; Huang, L.; Chen, J.; Li, J.J.; Wang, R.; Kim, E.; Chen, Y.; Justicia, C.; Sakata, K.; et al. A CNS-Permeable Hsp90 Inhibitor Rescues Synaptic Dysfunction and Memory Loss in APP-Overexpressing Alzheimer's Mouse Model via an HSF1-Mediated Mechanism. *Mol. Psychiatry* **2017**, *22*, 990–1001. [[CrossRef](#)] [[PubMed](#)]
- Aguilá, M.; Bevilacqua, D.; McCulley, C.; Schwarz, N.; Athanasiou, D.; Kanuga, N.; Novoselov, S.S.; Lange, C.A.K.; Ali, R.R.; Bainbridge, J.W.; et al. Hsp90 Inhibition Protects against Inherited Retinal Degeneration. *Hum. Mol. Genet.* **2014**, *23*, 2164–2175. [[CrossRef](#)]
- Stohtert, A.R.; Suntharalingam, A.; Tang, X.; Crowley, V.M.; Mishra, S.J.; Webster, J.M.; Nordhues, B.A.; Huard, D.J.E.; Passaglia, C.L.; Lieberman, R.L.; et al. Isoform-Selective Hsp90 Inhibition Rescues Model of Hereditary Open-Angle Glaucoma. *Sci. Rep.* **2017**, *7*, 17951. [[CrossRef](#)]
- Jaworski, T.; Banach-Kasper, E.; Gralec, K. GSK-3  $\beta$  at the Intersection of Neuronal Plasticity and Neurodegeneration. *Neural Plast.* **2019**, *2019*, 4209475. [[CrossRef](#)]
- Li, Y.-C.; Gao, W.-J. GSK-3 $\beta$  Activity and Hyperdopamine-Dependent Behaviors. *Neurosci. Biobehav. Rev.* **2011**, *35*, 645–654. [[CrossRef](#)]
- Huang, J.; Guo, X.; Li, W.; Zhang, H. Activation of Wnt/ $\beta$ -Catenin Signalling via GSK3 Inhibitors Direct Differentiation of Human Adipose Stem Cells into Functional Hepatocytes. *Sci. Rep.* **2017**, *7*, 40716. [[CrossRef](#)]
- Bharathy, N.; Svalina, M.N.; Settelmeier, T.P.; Cleary, M.M.; Berlow, N.E.; Airhart, S.D.; Xiang, S.; Keck, J.; Hayden, J.B.; Shern, J.F.; et al. Preclinical Testing of the Glycogen Synthase Kinase-3 $\beta$  Inhibitor Tideglusib for Rhabdomyosarcoma. *Oncotarget* **2017**, *8*, 62976–62983. [[CrossRef](#)]
- Arciniegas Ruiz, S.M.; Eldar-Finkelman, H. Glycogen Synthase Kinase-3 Inhibitors: Preclinical and Clinical Focus on CNS-A Decade Onward. *Front. Mol. Neurosci.* **2022**, *14*, 792364. [[CrossRef](#)]
- Zhao, Y.; Wang, C.; Wang, C.; Hong, X.; Miao, J.; Liao, Y.; Zhou, L.; Liu, Y. An Essential Role for Wnt/ $\beta$ -Catenin Signaling in Mediating Hypertensive Heart Disease. *Sci. Rep.* **2018**, *8*, 8996. [[CrossRef](#)] [[PubMed](#)]
- Custodio, R.J.P.; Kim, H.J.; Kim, J.; Ortiz, D.M.; Kim, M.; Buctot, D.; Sayson, L.V.; Lee, H.J.; Kim, B.-N.; Yi, E.C.; et al. Hippocampal Dentate Gyrus Proteomics Reveals Wnt Signaling Involvement in the Behavioral Impairment in the THRSP-Overexpressing ADHD Mouse Model. *Commun. Biol.* **2023**, *6*, 55. [[CrossRef](#)] [[PubMed](#)]
- Grünblatt, E.; Bartl, J.; Walitza, S. Methylphenidate Enhances Neuronal Differentiation and Reduces Proliferation Concomitant to Activation of Wnt Signal Transduction Pathways. *Transl. Psychiatry* **2018**, *8*, 51. [[CrossRef](#)] [[PubMed](#)]
- Grünblatt, E.; Nemoda, Z.; Werling, A.M.; Roth, A.; Angyal, N.; Tarnok, Z.; Thomsen, H.; Peters, T.; Hinney, A.; Hebebrand, J.; et al. The Involvement of the Canonical Wnt-signaling Receptor *LRP5* and *LRP6* Gene Variants with ADHD and Sexual Dimorphism: Association Study and Meta-analysis. *Am. J. Med. Genet. Part B Neuropsychiatr. Genet.* **2019**, *180*, 365–376. [[CrossRef](#)]

25. Walter, N.M.; Yde Ohki, C.M.; Rickli, M.; Smigielski, L.; Walitza, S.; Grünblatt, E. An Investigation on the Alterations in Wnt Signaling in ADHD across Developmental Stages. *Neurosci. Appl.* **2024**, *3*, 104070. [[CrossRef](#)]
26. Liang, E.F.; Lim, S.Z.; Tam, W.W.; Ho, C.S.; Zhang, M.W.; McIntyre, R.S.; Ho, R.C. The Effect of Methylphenidate and Atomoxetine on Heart Rate and Systolic Blood Pressure in Young People and Adults with Attention-Deficit Hyperactivity Disorder (ADHD): Systematic Review, Meta-Analysis, and Meta-Regression. *Int. J. Environ. Res. Public Health* **2018**, *15*, 1789. [[CrossRef](#)]
27. Daughton, J.M.; Kratochvil, C.J. Review of ADHD Pharmacotherapies: Advantages, Disadvantages, and Clinical Pearls. *J. Am. Acad. Child Adolesc. Psychiatry* **2009**, *48*, 240–248. [[CrossRef](#)]
28. Pliszka, S. Practice Parameter for the Assessment and Treatment of Children and Adolescents with Attention-Deficit/Hyperactivity Disorder. *J. Am. Acad. Child Adolesc. Psychiatry* **2007**, *46*, 894–921. [[CrossRef](#)]
29. Biederman, J.; Spencer, T.J. Psychopharmacological Interventions. *Child Adolesc. Psychiatr. Clin. N. Am.* **2008**, *17*, 439–458. [[CrossRef](#)]
30. Krishna Veni, N.; Karthika, D.; Surya Devi, M.; Rubini, M.F.; Vishalini, M.; Pradeepa, Y.J. Analysis of Monosodium L-Glutamate in Food Products by High-Performance Thin Layer Chromatography. *J. Young Pharm.* **2010**, *2*, 297–300. [[CrossRef](#)]
31. Shivasharan, B.D.; Nagakannan, P.; Thippeswamy, B.S.; Veerapur, V.P. Protective Effect of *Calendula officinalis* L. Flowers Against Monosodium Glutamate Induced Oxidative Stress and Excitotoxic Brain Damage in Rats. *Indian J. Clin. Biochem.* **2013**, *28*, 292–298. [[CrossRef](#)] [[PubMed](#)]
32. Mokhtar, H.I.; Abd El-Fadeal, N.M.; El-Sayed, R.M.; Hegazy, A.; El-Kherbetawy, M.K.; Hamad, A.G.; ElSayed, M.H.; Zaitone, S.A. Computational Analysis and Experimental Data Exploring the Role of Hesperetin in Ameliorating ADHD and SIRT1/Nrf2/Keap1/OH-1 Signaling. *Int. J. Mol. Sci.* **2024**, *25*, 9284. [[CrossRef](#)] [[PubMed](#)]
33. Salem, H.A.; Elsherbiny, N.; Alzahrani, S.; Alshareef, H.M.; Abd Elmageed, Z.Y.; Ajwah, S.M.; Hamdan, A.M.E.; Abdou, Y.S.; Galal, O.O.; El Azazy, M.K.A.; et al. Neuroprotective Effect of Morin Hydrate against Attention-Deficit/Hyperactivity Disorder (ADHD) Induced by MSG and/or Protein Malnutrition in Rat Pups: Effect on Oxidative/Monoamines/Inflammatory Balance and Apoptosis. *Pharmaceuticals* **2022**, *15*, 1012. [[CrossRef](#)] [[PubMed](#)]
34. Kesharwani, R.; Bhoumik, S.; Kumar, R.; Rizvi, S.I. Monosodium Glutamate Even at Low Dose May Affect Oxidative Stress, Inflammation and Neurodegeneration in Rats 2022. *Indian J. Clin. Biochem.* **2024**, *39*, 101–109. [[CrossRef](#)] [[PubMed](#)]
35. Asejeje, F.O.; Abiola, M.A.; Adeyemo, O.A.; Ogunro, O.B.; Ajayi, A.M. Exogenous Monosodium Glutamate Exacerbates Lipopolysaccharide-Induced Neurobehavioral Deficits, Oxidative Damage, Neuroinflammation, and Cholinergic Dysfunction in Rat Brain. *Neurosci. Lett.* **2024**, *825*, 137710. [[CrossRef](#)]
36. Jagetia, G.C.; Reddy, T.K. The Grapefruit Flavanone Naringin Protects against the Radiation-Induced Genomic Instability in the Mice Bone Marrow: A Micronucleus Study. *Mutat. Res. Toxicol. Environ. Mutagen.* **2002**, *519*, 37–48. [[CrossRef](#)]
37. Cavia-Saiz, M.; Busto, M.D.; Pilar-Izquierdo, M.C.; Ortega, N.; Perez-Mateos, M.; Muñoz, P. Antioxidant Properties, Radical Scavenging Activity and Biomolecule Protection Capacity of Flavonoid Naringenin and Its Glycoside Naringin: A Comparative Study. *J. Sci. Food Agric.* **2010**, *90*, 1238–1244. [[CrossRef](#)]
38. Eom, S.; Lee, B.-B.; Lee, S.; Park, Y.; Yeom, H.D.; Kim, T.-H.; Nam, S.-H.; Lee, J.H. Antioxidative and Analgesic Effects of Naringin through Selective Inhibition of Transient Receptor Potential Vanilloid Member 1. *Antioxidants* **2021**, *11*, 64. [[CrossRef](#)]
39. Long, J.; Chen, J.; Liao, Y.; Zhou, Y.; Liang, B.; Zhou, Y. Naringin Provides Neuroprotection in CCL2-Induced Cognition Impairment by Attenuating Neuronal Apoptosis in the Hippocampus. *Behav. Brain Funct.* **2020**, *16*, 4. [[CrossRef](#)]
40. Han, Y.; Su, J.; Liu, X.; Zhao, Y.; Wang, C.; Li, X. Naringin Alleviates Early Brain Injury after Experimental Subarachnoid Hemorrhage by Reducing Oxidative Stress and Inhibiting Apoptosis. *Brain Res. Bull.* **2017**, *133*, 42–50. [[CrossRef](#)]
41. Cui, J.; Wang, G.; Kandhare, A.D.; Mukherjee-Kandhare, A.A.; Bodhankar, S.L. Neuroprotective Effect of Naringin, a Flavone Glycoside in Quinolinic Acid-Induced Neurotoxicity: Possible Role of PPAR- $\gamma$ , Bax/Bcl-2, and Caspase-3. *Food Chem. Toxicol.* **2018**, *121*, 95–108. [[CrossRef](#)] [[PubMed](#)]
42. Karthikeyan, A.; Kim, H.H.; Preethi, V.; Moniruzzaman, M.; Lee, K.H.; Kalaiselvi, S.; Kim, G.S.; Min, T. Assessment of Anti-Inflammatory and Antioxidant Effects of Citrus Unshiu Peel (CUP) Flavonoids on LPS-Stimulated RAW 264.7 Cells. *Plants* **2021**, *10*, 2209. [[CrossRef](#)] [[PubMed](#)]
43. Akamo, A.J.; Akinloye, D.I.; Ugbaja, R.N.; Adeleye, O.O.; Dosumu, O.A.; Eteng, O.E.; Antiya, M.C.; Amah, G.; Ajayi, O.A.; Faseun, S.O. Naringin Prevents Cyclophosphamide-Induced Erythrocytotoxicity in Rats by Abrogating Oxidative Stress. *Toxicol. Rep.* **2021**, *8*, 1803–1813. [[CrossRef](#)] [[PubMed](#)]
44. Ahmed, S.; Khan, H.; Aschner, M.; Hasan, M.M.; Hassan, S.T.S. Therapeutic Potential of Naringin in Neurological Disorders. *Food Chem. Toxicol.* **2019**, *132*, 110646. [[CrossRef](#)] [[PubMed](#)]
45. Gentile, G.; Merlo, G.; Pozzan, A.; Bernasconi, G.; Bax, B.; Bamborough, P.; Bridges, A.; Carter, P.; Neu, M.; Yao, G.; et al. 5-Aryl-4-Carboxamide-1, 3-Oxazoles: Potent and Selective GSK-3 Inhibitors. *Bioorg. Med. Chem. Lett.* **2012**, *22*, 1989–1994. [[CrossRef](#)]
46. Tassone, G.; Mazzorana, M.; Mangani, S.; Petricci, E.; Cini, E.; Giannini, G.; Pozzi, C.; Maramai, S. Structural Characterization of Human Heat Shock Protein 90 N-Terminal Domain and Its Variants K112R and K112A in Complex with a Potent 1,2,3-Triazole-Based Inhibitor. *Int. J. Mol. Sci.* **2022**, *23*, 9458. [[CrossRef](#)]
47. Li, J.; Sun, L.; Xu, C.; Yu, F.; Zhou, H.; Zhao, Y.; Zhang, J.; Cai, J.; Mao, C.; Tang, L.; et al. Structure Insights into Mechanisms of ATP Hydrolysis and the Activation of Human Heat-Shock Protein 90. *Acta Biochim. Biophys. Sin.* **2012**, *44*, 300–306. [[CrossRef](#)]

48. Wang, H.; Liang, J.; Wang, Y.; Zheng, J.; Liu, Y.; Zhao, Y.; Ma, Y.; Chen, P.; Yang, X. Exploring the Effects of Naringin on Oxidative Stress-Impaired Osteogenic Differentiation via the Wnt/ $\beta$ -Catenin and PI3K/Akt Pathways. *Sci. Rep.* **2024**, *14*, 14047. [[CrossRef](#)]
49. Backe, S.J.; Heritz, J.A.; Mollapour, M. The HSP90 Chaperone Code Regulates the Crosstalk between Proteostasis and Autophagy. *Autophagy* **2024**, *20*, 1689–1691. [[CrossRef](#)]
50. Tharamelvelyil Rajendran, A.; Dheeraj Rajesh, G.; Ashtekar, H.; Sairam, A.; Kumar, P.; Vadakkepushpakath, A.N. Uncovering Naringin's Anticancer Mechanisms in Glioblastoma via Molecular Docking and Network Pharmacology Approaches. *Sci. Rep.* **2024**, *14*, 21486. [[CrossRef](#)]
51. Viswanathan, S.; Sivaraj, R.; Vasanthi, A.H.R.; Subramanian, K.; Ramesh, V. An In-Silico Approach—Molecular Docking Analysis of Flavonoids against GSK-3 $\beta$  and TNF- $\alpha$  Targets in Alzheimer's Disease. *J. Recept. Signal Transduct.* **2024**, 1–9. [[CrossRef](#)] [[PubMed](#)]
52. Rosso, S.B.; Inestrosa, N.C. WNT Signaling in Neuronal Maturation and Synaptogenesis. *Front. Cell. Neurosci.* **2013**, *7*, 103. [[CrossRef](#)] [[PubMed](#)]
53. Grove, E.A.; Tole, S.; Limon, J.; Yip, L.; Ragsdale, C.W. The Hem of the Embryonic Cerebral Cortex Is Defined by the Expression of Multiple *Wnt* Genes and Is Compromised in *Gli3*-Deficient Mice. *Development* **1998**, *125*, 2315–2325. [[CrossRef](#)] [[PubMed](#)]
54. Machon, O.; Van Den Bout, C.J.; Backman, M.; Kemler, R.; Krauss, S. Role of  $\beta$ -Catenin in the Developing Cortical and Hippocampal Neuroepithelium. *Neuroscience* **2003**, *122*, 129–143. [[CrossRef](#)] [[PubMed](#)]
55. Chodelkova, O.; Masek, J.; Korinek, V.; Kozmik, Z.; Machon, O. Tcf7L2 Is Essential for Neurogenesis in the Developing Mouse Neocortex. *Neural Develop.* **2018**, *13*, 8. [[CrossRef](#)]
56. Draganova, K.; Zemke, M.; Zurkirchen, L.; Valenta, T.; Cantù, C.; Okoniewski, M.; Schmid, M.-T.; Hoffmans, R.; Götz, M.; Basler, K.; et al. Wnt/ $\beta$ -Catenin Signaling Regulates Sequential Fate Decisions of Murine Cortical Precursor Cells. *Stem Cells* **2015**, *33*, 170–182. [[CrossRef](#)]
57. Ishii, K.; Furuta, T.; Kasuya, Y. Determination of Naringin and Naringenin in Human Plasma by High-Performance Liquid Chromatography. *J. Chromatogr. B. Biomed. Sci. App.* **1996**, *683*, 225–229. [[CrossRef](#)]
58. Heisler, J.M.; Morales, J.; Donegan, J.J.; Jett, J.D.; Redus, L.; O'Connor, J.C. The Attentional Set Shifting Task: A Measure of Cognitive Flexibility in Mice. *J. Vis. Exp.* **2015**, *96*, 51944. [[CrossRef](#)]
59. Swamy, R.S.; Kumar, N.; Shenoy, S.; Cheruku, S.P.; Rao, V.; Kumar, N.; Kumar, S.; Ravichandiran, V. Neuroprotective Effect by Naringin against Fluorosis-Induced Neurodegeneration in Adult Wistar Rats. *NeuroReport* **2023**, *34*, 449–456. [[CrossRef](#)]
60. Dai, X.; Jia, Y.; Cao, R.; Zhou, M. Naringin Prevents Cognitive Dysfunction in Aging Rats by Inhibiting Toll-Like Receptor 4 (TLR4)/NF- $\kappa$ B Pathway and Endoplasmic Reticulum Stress. *Evid.-Based Complement. Alternat. Med.* **2023**, *2023*, 2919811. [[CrossRef](#)]
61. Bauer, J.; Werner, A.; Kohl, W.; Kugel, H.; Shushakova, A.; Pedersen, A.; Ohrmann, P. Hyperactivity and Impulsivity in Adult Attention-Deficit/Hyperactivity Disorder Is Related to Glutamatergic Dysfunction in the Anterior Cingulate Cortex. *World J. Biol. Psychiatry* **2018**, *19*, 538–546. [[CrossRef](#)] [[PubMed](#)]
62. Huang, X.; Wang, M.; Zhang, Q.; Chen, X.; Wu, J. The Role of Glutamate Receptors in Attention-Deficit/Hyperactivity Disorder: From Physiology to Disease. *Am. J. Med. Genet. Part B Neuropsychiatr. Genet.* **2019**, *180*, 272–286. [[CrossRef](#)] [[PubMed](#)]
63. Alomar, S.Y.; Gheit, R.E.A.E.; Enan, E.T.; El-Bayoumi, K.S.; Shoaier, M.Z.; Elkazaz, A.Y.; Al Thagfan, S.S.; Zaitone, S.A.; El-Sayed, R.M. Novel Mechanism for Memantine in Attenuating Diabetic Neuropathic Pain in Mice via Downregulating the Spinal HMGB1/TRL4/NF- $\kappa$ B Inflammatory Axis. *Pharmaceuticals* **2021**, *14*, 307. [[CrossRef](#)]
64. Alomar, S.Y.; Barakat, B.M.; Eldosoky, M.; Atef, H.; Mohamed, A.S.; Elhawary, R.; El-Shafey, M.; Youssef, A.M.; Elkazaz, A.Y.; Gabr, A.M.; et al. Protective Effect of Metformin on Rat Diabetic Retinopathy Involves Suppression of Toll-like Receptor 4/Nuclear Factor- $\kappa$ B Expression and Glutamate Excitotoxicity. *Int. Immunopharmacol.* **2021**, *90*, 107193. [[CrossRef](#)]
65. Cheng, J.; Liu, A.; Shi, M.Y.; Yan, Z. Disrupted Glutamatergic Transmission in Prefrontal Cortex Contributes to Behavioral Abnormality in an Animal Model of ADHD. *Neuropsychopharmacology* **2017**, *42*, 2096–2104. [[CrossRef](#)] [[PubMed](#)]
66. Abu-Elfotuh, K.; Abdel-Sattar, S.A.; Abbas, A.N.; Mahran, Y.F.; Alshaniwani, A.R.; Hamdan, A.M.E.; Atwa, A.M.; Reda, E.; Ahmed, Y.M.; Zaghlool, S.S.; et al. The Protective Effect of Thymoquinone or/and Thymol against Monosodium Glutamate-Induced Attention-Deficit/Hyperactivity Disorder (ADHD)-like Behavior in Rats: Modulation of Nrf2/HO-1, TLR4/NF- $\kappa$ B/NLRP3/Caspase-1 and Wnt/ $\beta$ -Catenin Signaling Pathways in Rat Model. *Biomed. Pharmacother.* **2022**, *155*, 113799. [[CrossRef](#)]
67. Ilgin, N.; Senol, S.; Gucuyener, K.; Gokcora, N.; Atavci, S.; Sener, S. Is Increased D2 Receptor Availability Associated with Response to Stimulant Medication in ADHD. *Dev. Med. Child Neurol.* **2001**, *43*, 755. [[CrossRef](#)]
68. Volkow, N.D.; Wang, G.-J.; Newcorn, J.; Fowler, J.S.; Telang, F.; Solanto, M.V.; Logan, J.; Wong, C.; Ma, Y.; Swanson, J.M.; et al. Brain Dopamine Transporter Levels in Treatment and Drug Naïve Adults with ADHD. *NeuroImage* **2007**, *34*, 1182–1190. [[CrossRef](#)]
69. Stahl, S.M.; Pradko, J.; Haight, B.R.; Modell, J.G.; Rockett, C.B.; Learned-Coughlin, S. A Review of the Neuropharmacology of Bupropion, a Dual Norepinephrine and Dopamine Reuptake Inhibitor. *Prim. Care Companion CNS Disord.* **2004**, *6*, 159. [[CrossRef](#)]
70. Zimmer, L. Contribution of Clinical Neuroimaging to the Understanding of the Pharmacology of Methylphenidate. *Trends Pharmacol. Sci.* **2017**, *38*, 608–620. [[CrossRef](#)]
71. Faraone, S.V. The Pharmacology of Amphetamine and Methylphenidate: Relevance to the Neurobiology of Attention-Deficit/Hyperactivity Disorder and Other Psychiatric Comorbidities. *Neurosci. Biobehav. Rev.* **2018**, *87*, 255–270. [[CrossRef](#)] [[PubMed](#)]



72. Llorente, A.M.; Voigt, R.G.; Jensen, C.L.; Berretta, M.C.; Kennard Fraley, J.; Heird, W.C. Performance on a Visual Sustained Attention and Discrimination Task Is Associated with Urinary Excretion of Norepinephrine Metabolite in Children with Attention-Deficit/Hyperactivity Disorder (AD/HD). *Clin. Neuropsychol.* **2006**, *20*, 133–144. [[CrossRef](#)]
73. Weißflog, L.; Scholz, C.-J.; Jacob, C.P.; Nguyen, T.T.; Zamzow, K.; Groß-Lesch, S.; Renner, T.J.; Romanos, M.; Rujescu, D.; Walitza, S.; et al. KCNIP4 as a Candidate Gene for Personality Disorders and Adult ADHD. *Eur. Neuropsychopharmacol.* **2013**, *23*, 436–447. [[CrossRef](#)] [[PubMed](#)]
74. Wiese, K.E.; Nusse, R.; Van Amerongen, R. Wnt Signalling: Conquering Complexity. *Development* **2018**, *145*, dev165902. [[CrossRef](#)] [[PubMed](#)]
75. Nusse, R.; Clevers, H. Wnt/ $\beta$ -Catenin Signaling, Disease, and Emerging Therapeutic Modalities. *Cell* **2017**, *169*, 985–999. [[CrossRef](#)]
76. Rubio, C.; Rosiles-Abonce, A.; Trejo-Solis, C.; Rubio-Osornio, M.; Mendoza, C.; Custodio, V.; Martinez-Lazcano, J.C.; Gonzalez, E.; Paz, C. Increase Signaling of Wnt/ $\beta$ -Catenin Pathway and Presence of Apoptosis in Cerebellum of Kindled Rats. *CNS Neurol. Disord.-Drug Targets* **2017**, *16*, 772–780. [[CrossRef](#)]
77. De Ferrari, G.V.; Chacón, M.A.; Barriá, M.I.; Garrido, J.L.; Godoy, J.A.; Olivares, G.; Reyes, A.E.; Alvarez, A.; Bronfman, M.; Inestrosa, N.C. Activation of Wnt Signaling Rescues Neurodegeneration and Behavioral Impairments Induced by  $\beta$ -Amyloid Fibrils. *Mol. Psychiatry* **2003**, *8*, 195–208. [[CrossRef](#)]
78. Ye, X.; Zerlanko, B.; Kennedy, A.; Banumathy, G.; Zhang, R.; Adams, P.D. Downregulation of Wnt Signaling Is a Trigger for Formation of Facultative Heterochromatin and Onset of Cell Senescence in Primary Human Cells. *Mol. Cell* **2007**, *27*, 183–196. [[CrossRef](#)]
79. Acebron, S.P.; Niehrs, C.  $\beta$ -Catenin-Independent Roles of Wnt/LRP6 Signaling. *Trends Cell Biol.* **2016**, *26*, 956–967. [[CrossRef](#)]
80. Caracci, M.O.; Avila, M.E.; Espinoza-Cavieles, F.A.; López, H.R.; Ugarte, G.D.; De Ferrari, G.V. Wnt/ $\beta$ -Catenin-Dependent Transcription in Autism Spectrum Disorders. *Front. Mol. Neurosci.* **2021**, *14*, 764756. [[CrossRef](#)]
81. Fakhri, S.; Abbaszadeh, F.; Dargahi, L.; Jorjani, M. Astaxanthin: A Mechanistic Review on Its Biological Activities and Health Benefits. *Pharmacol. Res.* **2018**, *136*, 1–20. [[CrossRef](#)] [[PubMed](#)]
82. Yang, W.; Ma, J.; Liu, Z.; Lu, Y.; Hu, B.; Yu, H. Effect of Naringenin on Brain Insulin Signaling and Cognitive Functions in ICV-STZ Induced Dementia Model of Rats. *Neurol. Sci.* **2014**, *35*, 741–751. [[CrossRef](#)] [[PubMed](#)]
83. Zhang, N.; Hu, Z.; Zhang, Z.; Liu, G.; Wang, Y.; Ren, Y.; Wu, X.; Geng, F. Protective Role Of Naringenin Against A $\beta$ 25-35-Caused Damage via ER and PI3K/Akt-Mediated Pathways. *Cell. Mol. Neurobiol.* **2018**, *38*, 549–557. [[CrossRef](#)] [[PubMed](#)]
84. Ghofrani, S.; Joghataei, M.-T.; Mohseni, S.; Baluchnejadmojarad, T.; Bagheri, M.; Khamse, S.; Roghani, M. Naringenin Improves Learning and Memory in an Alzheimer's Disease Rat Model: Insights into the Underlying Mechanisms. *Eur. J. Pharmacol.* **2015**, *764*, 195–201. [[CrossRef](#)] [[PubMed](#)]
85. Affany, A.; Salvayre, R.; Douste-Blazy, L. Comparison of the Protective Effect of Various Flavonoids Against Lipid Peroxidation of Erythrocyte Membranes (Induced by Cumene Hydroperoxide). *Fundam. Clin. Pharmacol.* **1987**, *1*, 451–457. [[CrossRef](#)]
86. Korkina, L.G.; Afanas'Ev, I.B. Antioxidant and Chelating Properties of Flavonoids. In *Advances in Pharmacology*; Elsevier: Amsterdam, The Netherlands, 1996; Volume 38, pp. 151–163. ISBN 978-0-12-032939-7.
87. Chen, Y.; Zheng, R.; Jia, Z.; Ju, Y. Flavonoids as Superoxide Scavengers and Antioxidants. *Free Radic. Biol. Med.* **1990**, *9*, 19–21. [[CrossRef](#)]
88. Russo, A.; Acquaviva, R.; Campisi, A.; Sorrenti, V.; Di Giacomo, C.; Virgata, G.; Barcellona, M.L.; Vanella, A. Bioflavonoids as antiradicals, antioxidants and DNA cleavage protectors. *Cell Biol. Toxicol.* **2000**, *16*, 91–98. [[CrossRef](#)]
89. Alvarez-González, I.; Madrigal-Bujaidar, E.; Dorado, V.; Espinosa-Aguirre, J.J. Inhibitory Effect of Naringin on the Micronuclei Induced by Ifosfamide in Mouse, and Evaluation of Its Modulatory Effect on the Cyp3a Subfamily. *Mutat. Res./Fundam. Mol. Mech. Mutagen.* **2001**, *480–481*, 171–178. [[CrossRef](#)]
90. Abd-Elmawla, M.A.; Essam, R.M.; Ahmed, K.A.; Abdelmonem, M. Implication of Wnt/GSK-3 $\beta$ / $\beta$ -Catenin Signaling in the Pathogenesis of Mood Disturbances Associated with Hyperthyroidism in Rats: Potential Therapeutic Effect of Naringin. *ACS Chem. Neurosci.* **2023**, *14*, 2035–2048. [[CrossRef](#)]
91. Yuan, Z.; Yang, Z. The Effect of Naringin on the Apoptosis of Degenerative Nucleus Pulposus Cells: A Study on the Function and Mechanism. *Drug Des. Devel. Ther.* **2022**, *16*, 499–508. [[CrossRef](#)]
92. McGann, M. FRED Pose Prediction and Virtual Screening Accuracy. *J. Chem. Inf. Model.* **2011**, *51*, 578–596. [[CrossRef](#)]
93. Kanehisa, M.; Sato, Y.; Kawashima, M.; Furumichi, M.; Tanabe, M. KEGG as a reference resource for gene and protein annotation. *Nucleic acids research* **2016**, *44*, D457–D462. [[CrossRef](#)] [[PubMed](#)]
94. Onaolapo, A.Y.; Odetunde, I.; Akintola, A.S.; Ogundeji, M.O.; Ajao, A.; Obelawo, A.Y.; Onaolapo, O.J. Dietary Composition Modulates Impact of Food-Added Monosodium Glutamate on Behaviour, Metabolic Status and Cerebral Cortical Morphology in Mice. *Biomed. Pharmacother.* **2019**, *109*, 417–428. [[CrossRef](#)] [[PubMed](#)]
95. Termkwancharoen, C.; Malakul, W.; Phetrungnapha, A.; Tunsophon, S. Naringin Ameliorates Skeletal Muscle Atrophy and Improves Insulin Resistance in High-Fat-Diet-Induced Insulin Resistance in Obese Rats. *Nutrients* **2022**, *14*, 4120. [[CrossRef](#)] [[PubMed](#)]
96. Meikle, L.; Pollizzi, K.; Egnor, A.; Kramvis, I.; Lane, H.; Sahin, M.; Kwiatkowski, D.J. Response of a Neuronal Model of Tuberous Sclerosis to Mammalian Target of Rapamycin (mTOR) Inhibitors: Effects on mTORC1 and Akt Signaling Lead to Improved Survival and Function. *J. Neurosci.* **2008**, *28*, 5422–5432. [[CrossRef](#)] [[PubMed](#)]

97. Soltani, Z.; Shariatpanahi, M.; Aghsami, M.; Owliaey, H.; Kheradmand, A. Investigating the Effect of Exposure to Monosodium Glutamate during Pregnancy on Development of Autism in Male Rat Offspring. *Food Chem. Toxicol.* **2024**, *185*, 114464. [[CrossRef](#)]
98. Yu, T.; Zhao, Y.; Shi, W.; Ma, R.; Yu, L. Effects of Maternal Oral Administration of Monosodium Glutamate at a Late Stage of Pregnancy on Developing Mouse Fetal Brain. *Brain Res.* **1997**, *747*, 195–206. [[CrossRef](#)]
99. Birrell, J.M.; Brown, V.J. Medial Frontal Cortex Mediates Perceptual Attentional Set Shifting in the Rat. *J. Neurosci.* **2000**, *20*, 4320–4324. [[CrossRef](#)]
100. El-Sherbeeney, N.A.; Soliman, N.; Youssef, A.M.; Abd El-Fadeal, N.M.; El-Abaseri, T.B.; Hashish, A.A.; Abdelbasset, W.K.; El-Saber Batiha, G.; Zaitone, S.A. The Protective Effect of Biochanin A against Rotenone-Induced Neurotoxicity in Mice Involves Enhancing of PI3K/Akt/mTOR Signaling and Beclin-1 Production. *Ecotoxicol. Environ. Saf.* **2020**, *205*, 111344. [[CrossRef](#)]
101. Livak, K.J.; Schmittgen, T.D. Analysis of Relative Gene Expression Data Using Real-Time Quantitative PCR and the  $2^{-\Delta\Delta CT}$  Method. *Methods* **2001**, *25*, 402–408. [[CrossRef](#)]
102. Elsherbiny, N.M.; Abdel-Mottaleb, Y.; Elkazaz, A.Y.; Atef, H.; Lashine, R.M.; Youssef, A.M.; Ezzat, W.; El-Ghaiesh, S.H.; Elshaer, R.E.; El-Shafey, M.; et al. Carbamazepine Alleviates Retinal and Optic Nerve Neural Degeneration in Diabetic Mice via Nerve Growth Factor-Induced PI3K/Akt/mTOR Activation. *Front. Neurosci.* **2019**, *13*, 1089. [[CrossRef](#)] [[PubMed](#)]
103. Bahr, H.I.; Toraih, E.A.; Mohammed, E.A.; Mohammad, H.M.F.; Ali, E.A.I.; Zaitone, S.A. Chemopreventive Effect of Leflunomide against Ehrlich's Solid Tumor Grown in Mice: Effect on EGF and EGFR Expression and Tumor Proliferation. *Life Sci.* **2015**, *141*, 193–201. [[CrossRef](#)] [[PubMed](#)]
104. Ali, S.A.; Zaitone, S.A.; Moustafa, Y.M. Boswellic Acids Synergize Antitumor Activity and Protect against the Cardiotoxicity of Doxorubicin in Mice Bearing Ehrlich's Carcinoma. *Can. J. Physiol. Pharmacol.* **2015**, *93*, 695–708. [[CrossRef](#)] [[PubMed](#)]

**Disclaimer/Publisher's Note:** The statements, opinions and data contained in all publications are solely those of the individual author(s) and contributor(s) and not of MDPI and/or the editor(s). MDPI and/or the editor(s) disclaim responsibility for any injury to people or property resulting from any ideas, methods, instructions or products referred to in the content.